TNO Built Environment and Geosciences

Princetonlaan 6
P.O. Box 80015
3508 TA Utrecht
The Netherlands

www.tno.nl

T +31 30 256 42 56
F +31 30 256 44 75
info-BenO@tno.nl

TNO report

TNO-034-UT-2009-02410

Lower Cretaceous Rijnland Group aquifers in the West Netherlands Basin: suitability for geothermal energy

Date	6 May 2010
Author(s)	dr. G.-J. Vis, drs. S.F. van Gessel, drs. H.F. Mijnlieff, drs. M.P.D. Pluymaekers, ing. J.M.M. Hettelaar, D.P.M. Stegers M.Sc.
Assignor	Ministry of Economic Affairs
Project number	034.20776/01.02

Classification report
Title
Abstract
Report text
Appendices

Number of pages	55 (incl. appendices)
Number of appendices	14 (incl. 12 maps)

All rights reserved. No part of this report may be reproduced and/or published in any form by print, photoprint, microfilm or any other means without the previous written permission from TNO.

All information which is classified according to Dutch regulations shall be treated by the recipient in the same way as classified information of corresponding value in his own country. No part of this information will be disclosed to any third party.

In case this report was drafted on instructions, the rights and obligations of contracting parties are subject to either the Standard Conditions for Research Instructions given to TNO, or the relevant agreement concluded between the contracting parties. Submitting the report for inspection to parties who have a direct interest is permitted.

© 2010 TNO

Proclaimer

NEDERLANDS:
De resultaten en kaarten in dit rapport zijn gebaseerd op een regionale kartering van de ondergrond van het West Nederlands Bekken. De resultaten en kaarten zijn verkregen met een grootschalige modelleerstudie van geologische parameters in de bestudeerde aquifers. Daarom dienen de resultaten en kaarten in dit rapport uitsluitend gebruikt te worden voor regionale geologische evaluaties. De resultaten en kaarten in dit rapport dienen niet gebruikt te worden voor lokale aardwarmtestudies. Tevens dienen de resultaten en kaarten in dit rapport niet gebruikt te worden voor bedrijfsmatige doeleinden.

De resultaten en kaarten in dit rapport zijn met grote zorg samengesteld. Ondanks deze zorgvuldigheid is het mogelijk dat de gepresenteerde informatie onvolledigheden, onjuistheden of fouten bevat. Daarnaast is het mogelijk dat voortschrijdend inzicht en nieuwe gegevens ervoor zorgen dat een gedeelte van de gepresenteerde resultaten en kaarten op termijn niet meer geheel actueel is. TNO is niet verantwoordelijk voor eventuele fouten of andere consequenties die het gevolg zijn van het gebruik van de resultaten en kaarten in dit rapport.

ENGLISH:
The results and maps in this report are based on regional geological mapping of the West Netherlands Basin. The results and maps were generated by a large-scale modelling study of geological parameters of the studied aquifers. Therefore, the results and maps of this report should only be used for regional geological evaluations. The results and maps in this report should not be used for local geothermal studies and commercial purposes.

The results and maps in this report have been carefully compiled. Nonetheless the presented results may contain incomplete, incorrect or erroneous information. Furthermore, advances in knowledge and new data may cause some results and maps to become out of date. TNO claims to be not responsible for any eventual errors or other consequences resulting from the use of the results and maps in this report.

Samenvatting

Het doel van deze studie is het modelleren in 3D van de ruimtelijke verdeling van porositeit en permeabiliteit (transmissiviteit = netto zanddikte · permeabiliteit) in de Onder Krijt Rijnland Group van het West Nederlands Bekken, met het oog op de toepassing voor aardwarmtewinning. De studie is gebaseerd op de gemodelleerde 3D verdeling van zand lithofacies (aquifers) van de Rijnland Groep en maakt gebruik van putten en seismiek uit het publieke domein (DINO database bij TNO). Er is gebruik gemaakt van *gamma ray* logs om aquifers in de Rijnland Groep te identificeren. Op basis van deze logs, is een 3D lithofacies model gemaakt van de Rijnland Groep als geheel op basis van 50 stochastische modelrealisaties. Porositeitslogs zijn berekend met behulp van *bulk density* en *neutron* logs en kernplugmetingen van porositeit en permeabiliteit. De porositeitslogs zijn gebruikt om een 3D porositeitsmodel te berekenen op basis van 50 stochastische modelrealisaties. Permeabiliteitslogs zijn berekend op basis van de lineaire relatie tussen porositeit en de natuurlijke logaritme van permeabiliteit (*ln*K) op basis van kernplugmetingen per put en per aquifer. Met behulp van de parameters van het verband tussen porositeit en permeabiliteit per put, is een 3D permeabiliteitsmodel gemaakt op basis van 50 verschillende stochastische realisaties. Dit model is vervolgens gebruikt om transmissiviteitskaarten te berekenen voor het gehele Rijnland Groep interval in het West Nederlands Bekken. Verder zijn kaarten met de verwachte netto zanddikte en netto porositeit berekend op.

De resultaten van deze studie laten zien dat de ruimtelijke verdeling van aquifers in het 3D model van de Rijnland Groep consistent is met algemene geologische concepten en putgegevens voor het West Nederlands Bekken (betreffende stratigrafische dikte en laterale uitbreiding). De netto zanddikte (aquifer dikte) in het West Nederlands Bekken is sterk gecorreleerd met de gehele dikte van de Rijnland Groep. De verwachte netto aquifer dikte is het grootst in het centrale deel van het bekken ($\leq$ 500 m) tussen de steden Den Haag, Rotterdam en Gouda. De grootste netto aquifer dikte komt overeen met de grootste onzekerheid in dikte, als gevolg van de beperkte hoeveelheid putgegevens in de grabens van het bekken. Doordat de netto aquifer dikte het grootst is in het centrale deel van het bekken, zijn verwachte netto transmissiviteitswaarden het hoogst in die regio (wanneer het gehele Rijnland Groep interval wordt doorboord). Ten tijde van afzetting werd de verdeling van facies in het West Nederlands Bekken waarschijnlijk voornamelijk gestuurd door de balans tussen (relatieve) zeespiegelstijging en sediment aanvoer door rivieren.

Over het algemeen kan geconcludeerd worden dat de Rijnland Groep in het West Nederlands Bekken zeer geschikt is voor aardwarmtewinning. Dit geldt vooral voor het gebied tussen de steden Den Haag, Rotterdam en Gouda.

Summary

This study aims at 3D modelling of the spatial distribution of porosity and permeability (transmissivity = net sand thickness · permeability) in the Lower Cretaceous Rijnland Group in the West Netherlands Basin with respect to the applicability for geothermal energy production. The modelling is based on the modelled 3D distribution of sand lithofacies (aquifers) and based on public well and seismic data originating from the DINO database at TNO *Geological Survey of the Netherlands*. Gamma ray logs were used to identify aquifer intervals in the Rijnland Group. Based on these logs, a 3D lithofacies model was made of the entire Rijnland Group interval, based on 50 stochastic realisations. Porosity logs were calculated using bulk density and neutron logs, and core plug measurements. The porosity logs were used to calculate a 3D porosity model based on 50 stochastic model realisations. Permeability logs were calculated using the linear relationship between porosity and the natural logarithm of permeability (*ln*K) in core plug measurements for each well and aquifer. Using the parameters of the linear relationship between porosity and permeability for each well, a 3D permeability model was generated based on 50 stochastic model realisations. The 3D model was used to produce transmissivity maps for the entire Rijnland Group interval in the West Netherlands Basin. Furthermore, maps of the expected net sand thickness and net porosity distribution were created.

The results of this study show that the spatial distribution of aquifers in the 3D model of the Rijnland Group is consistent with general geological concepts and well data for the West Netherlands Basin (in terms of stratigraphic thickness and lateral extent). The net sand (aquifer) thickness in the West Netherlands Basin is strongly correlated with the complete thickness of the Rijnland Group. The summed thickness of aquifers is expected to be thickest in the central part of the basin ($\leq$ 500 m) between the cities of Den Haag, Rotterdam and Gouda. The largest net aquifer thickness corresponds with the highest uncertainty of thickness due to limited well-control in the grabens of the basin. Because of the largest net aquifer thickness in the central part of the basin, net transmissivity values are expected to be highest in that region, when penetrating the complete Rijnland Group interval. The distribution of facies during deposition in the West Netherlands Basin was most likely controlled by the balance between (relative) sea-level rise and fluvial sediment supply.

In general it can be concluded that the Rijnland Group in the West Netherlands Basin is well suited for geothermal energy production. Most suited is the central part of the basin between the cities of Den Haag, Rotterdam and Gouda.

Contents

1	**Introduction**	**7**
1.1	Background	7
1.2	Study focus	7
1.3	Study area and regional setting	9
2	**Methods**	**12**
2.1	Dataset	12
2.2	Well data processing	12
2.2.1	Lithofacies	12
2.2.2	Porosity logs	13
2.2.3	Permeability logs	15
2.3	Modelling assumptions	16
2.3.1	Sedimentary architecture	16
2.3.2	Chronology	16
2.3.3	Porosity-permeability relationships	17
2.4	Modelling workflow	18
2.4.1	3D grid model	19
2.4.2	Upscaling	19
2.4.3	Lithofacies modelling	20
2.4.4	Porosity modelling	20
2.4.5	Permeability modelling	23
3	**Results and discussion**	**26**
3.1	3D models	26
3.1.1	Lithofacies model and net sand maps	26
3.1.2	Porosity model and net porosity maps	29
3.1.3	Permeability model and net transmissivity maps	29
3.2	Geological insights	31
3.3	Applicability of WNB deposits for geothermal energy	33
4	**Conclusions and recommendations**	**34**
5	**References**	**36**
6	**Signature**	**38**

Appendices

Appendix 1: 538 available wells
Appendix 2: facies analysis
Map 1A: net sand lithofacies thickness map (P10) of the Rijnland Group in the West Netherlands Basin
Map 1B: net sand lithofacies thickness map (P50) of the Rijnland Group in the West Netherlands Basin
Map 1C: net sand lithofacies thickness map (P90) of the Rijnland Group in the West Netherlands Basin
Map 1D: net sand lithofacies thickness map (P10-P90) of the Rijnland Group in the West Netherlands Basin
Map 2A: net porosity map (P10) of the Rijnland Group in the West Netherlands Basin
Map 2B: net porosity map (P50) of the Rijnland Group in the West Netherlands Basin
Map 2C: net porosity map (P90) of the Rijnland Group in the West Netherlands Basin
Map 2D: net porosity map (P10-P90) of the Rijnland Group in the West Netherlands Basin
Map 3A: net transmissivity map (P10) of the Rijnland Group in the West Netherlands Basin
Map 3B: net transmissivity map (P50) of the Rijnland Group in the West Netherlands Basin
Map 3C: net transmissivity map (P90) of the Rijnland Group in the West Netherlands Basin
Map 3D: net transmissivity map (P10-P90) of the Rijnland Group in the West Netherlands Basin

1 Introduction

1.1 Background

The rising energy prices and the growing awareness of human impact on global climate have led to a growing interest in geothermal energy (Fridleifsson, et al., 2008; Solomon, et al., 2007). In the Netherlands this is expressed by the number of geothermal licence applications, which has grown to 57 during the last years (www.nlog.nl, December 2009). The majority of these applications are concentrated in the agricultural greenhouse district in the southwest of the Dutch province of Zuid-Holland (Fig. 1). Here, suitable Lower Cretaceous aquifers with a temperature above ~40°C are situated at depths below 1-2 km (NITG, 2002). Therefore, most of the geothermal licence applications in this region currently aim for the Late Mesozoic aquifers in the West Netherlands Basin (WNB).

In the WNB the presence of hydrocarbons was first proven by an exploration well in The Hague in 1938 (NITG, 2002). Since then exploration of the WNB commenced and until the present day the Nederlandse Aardolie Maatschappij (NAM) holds the production licence (Rijswijk concession) for the entire onshore part of the WNB (Fig. 1). Offshore, besides NAM, Cirrus and Delta hold exploration and production licences in the WNB. Currently oil and gas are being produced from about 55 wells from Triassic, Jurassic and Cretaceous reservoirs (www.nlog.nl, April 2010). The first exploration wells for geothermal energy in the WNB were successfully drilled in 2006-2007 (VDB-01 & VDB-02), targeting a Lower Cretaceous aquifer.

The recent interest in the WNB with respect to geothermal energy is a reason for renewed geological research. The present study aims to improve the understanding of the spatial distribution of Lower Cretaceous aquifers from the Rijnland Group (Van Adrichem Boogaert and Kouwe, 1993) in the WNB and their suitability for geothermal energy exploitation. The important parameters for geothermal energy production are porosity (PHI, in %), permeability (K, in mD) and transmissivity (Kh, in Dm). Therefore, this study specifically aims at *modelling* the spatial distribution of porosity and permeability (transmissivity) based on the *modelled* 3D distribution of sand lithofacies in the Rijnland Group. Modelling is based on public well and seismic data originating from the DINO database at TNO.

Besides publication in this report, the data from this study will be incorporated in the newly developed ThermoGIS^{TM} application, which is due to be launched in May 2010 (report TNO-034-UT-2010-00474/A). Furthermore, the results have been used for a study which results in recommendations for measures to improve geothermal energy production in the Netherlands (report TNO-034-UT-2010-00473/A).

1.2 Study focus

The present study focuses on facies and property modelling of the Rijnland Group. The coastal facies of this group have a relatively robust character (Dutch: *robuust*), because—although narrow—they mainly consist of laterally extensive deposits.

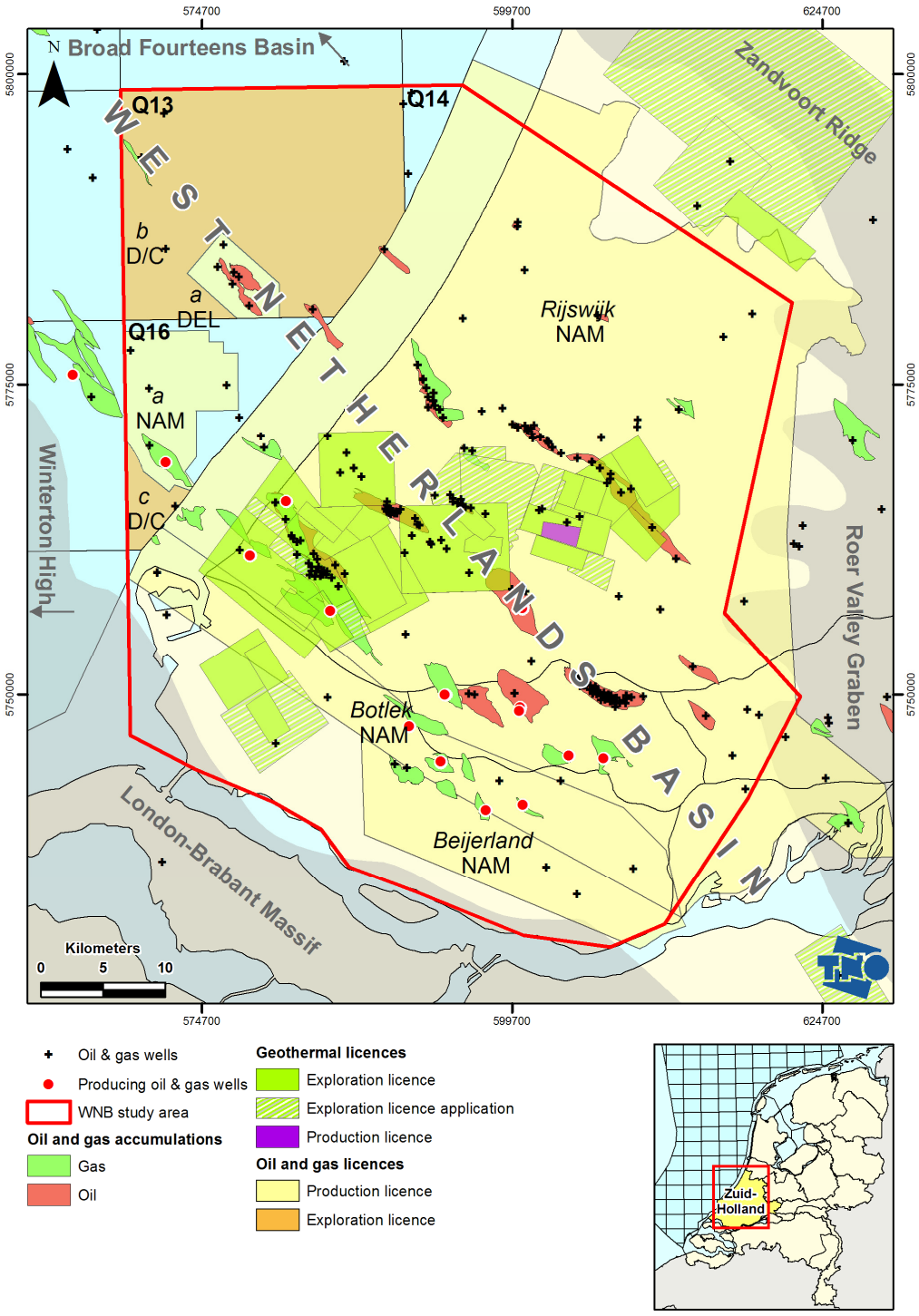

Figure 1. Study area in the southwest of the Netherlands (province of Zuid-Holland). Gray indicates structural elements other than the West Netherlands Basin (WNB). Exploration licences: NAM = Nederlandse Aardolie Maatschappij, CIR = Cirrus, DEL = Delta, D/C = Delta & Cirrus. European Datum 1950, UTM Zone 31N.

Furthermore, there is a relatively large amount of well data from the Rijnland Group due to oil and gas exploration.

The Schieland Group which underlies the Rijnland Group, has not been modelled in this study because facies and property modelling is hampered by:

1. A limited amount of well data;
2. A concentration of well data on elevated tectonic blocks (i.e. a poor spatial distribution) and very limited well data in the subsiding depressions, where syn-depositional rifting has occurred. This caused the main channels to be confined in subsiding depressions, which resulted in strong thickness variations in the Schieland Group (Den Hartog Jager, 1996; DeVault and Jeremiah, 2002);
3. The irregular, discontinuous and elongated fluvial braided to meandering deposits, creating an erratic character of the subsurface (Dutch: *grillig*).

Modelled facies distributions will largely depend on pre-defined conceptual models leading to a possible underestimation of the amount of sand layers (aquifers) in the Rodenrijs Claystone and the Alblasserdam Members. Because of the increasing interest in the Schieland Group aquifers, a regional study based on the available data and literature-based geological concepts is urgently needed.

1.3 Study area and regional setting

The study area is limited to the spatial extent of the Lower Cretaceous Rijnland Group deposits in the southwest of the Netherlands. In the offshore section of the WNB the limits have been set at the boundaries of the blocks Q13, Q14 and Q16 (Fig. 1).

The large amount of oil and gas fields in the WNB has led to numerous geological studies of this sedimentary basin (e.g. Alberts, et al., 2003; De Jager, et al., 1996; Den Hartog Jager, 1996; Gras and Geluk, 1999; Racero-Baena and Drake, 1996; Van Balen, et al., 2000). However, the generally poor quality of older well logs and 3D seismic data, the structural complexity, the preferential occurrence of oil and gas in uplifted fault blocks, and the decreased geological interest during the last five to ten years, have resulted in a fragmentary understanding of the sedimentary geology of the WNB.

The WNB is a basin in the southern North Sea Basin which experienced polyphase tectonic deformation since the Late Carboniferous (e.g. Dronkers and Mrozek, 1991; Heybroek, 1974; Van Wijhe, 1987; Ziegler, 1990). The basin is surrounded by the London-Brabant Massif to the south, the Winterton High to the west and the Zandvoort Ridge to the north. Towards the southeast the basin borders the Roer Valley Graben and towards the northwest it is connected with the Broad Fourteens Basin (Fig. 1). The Late Carboniferous to Tertiary tectonic history can be subdivided into four stages (Van Balen, et al., 2000; Van Wees, et al., 2009; Worum, et al., 2005):

- *Late Carboniferous-Early Permian stage*: the basin experienced strong subsidence since the Namurian (Langenaeker, 1998). During the Variscan orogeny, from the Westphalian D to the Early Permian, uplift and erosion took place. Uplift in the south of the basin was less strong than in the north. The Late Carboniferous basin was filled with mainly fine-grained deposits;
- *Late Permian-Middle Jurassic pre-rift stage*: the WNB formed a stable block during the Late Permian, until the ultimate stage of the Late Permian when the

basin was uplifted during a rift pulse. During the Early Triassic the WNB was characterized by regional thermal subsidence. At the end of the Early Triassic, during the Hardegsen phase, the northern part of the basin was uplifted (Geluk, et al., 1996). The Middle to Late Triassic development was characterized by tectonic movements of the Early Kimmerian tectonic phase. The WNB now formed a structurally simple large-scale half-graben, bounded by a major fault zone in the north (Geluk, 1999). The Early Kimmerian phase resulted in a large intra Triassic hiatus in the WNB. Since the Late Triassic differential subsidence has been observed. Around the Middle Jurassic, during the Mid Kimmerian tectonic phase, uplift resulted in erosion and the formation of an unconformity (Herngreen, et al., 2003). This unconformity corresponds with the base of the Schieland Group in the WNB;

- *Late Jurassic-Early Cretaceous syn-rift stage*: during this period the strongest rifting occurred during the Late Kimmerian tectonic phase (De Jager, et al., 1996; Racero-Baena and Drake, 1996; Van Wijhe, 1987). This resulted in the breaking-up of the basin in several subunits, causing variable thicknesses of the Late Jurassic infill. Within the Schieland Group – Nieuwerkerk Formation, a major unconformity has been identified (K35 Tectonic Boundary), marking the last phase of syn-rift movement (DeVault and Jeremiah, 2002). Superimposed on the tectonic movements is a period of global eustatic sea level-rise (Haq, et al., 1987). Rifting gradually stopped during the later part of the Early Cretaceous, but subsidence continued until this time (Van Wijhe, 1987);
- *Late Cretaceous-Quaternary post-rift and inversion stages*: during the middle of the Late Cretaceous, collision of the European and African plates and active spreading of Atlantic and Arctic mid-oceanic ridges, resulted in N-S regional compression and inversion (NITG, 2002; Van Wijhe, 1987). The inversion reactivated major fault zones, which show reverse movements. Many of the oil-bearing structures were formed during this period (e.g. De Jager, et al., 1996). Due to the inversion, pronounced uplift occurred and (Rijnland Group) sediments deposited in former depocentres were partially eroded. Around the end of the Late Cretaceous inversion movements ended and the entire WNB was covered by renewed sedimentation. During the Tertiary renewed uplift occurred, causing erosion of most of the sediments deposited during the Paleogene. Since the onset of the Neogene period (last 25 Ma), the WNB is subsiding.

Due to the tectonic history of the basin, the structural framework has a complex nature with many NW-SE trending faults, horsts and grabens. The main sedimentary deposits in the WNB belong to the continental Schieland Group and the marine Rijnland Group. These two groups are largely time-equivalent (Fig. 2). The Schieland Group consists of sandy fluvial channel deposits in a shaley lacustrine overbank environment. Due to syn-sedimentary fault movements, the thickness of this group is highly variable, being thickest (≤1600 m) in the grabens (DeVault and Jeremiah, 2002; NITG, 2002). The Rijnland Group consists of sandy marine transgressive deposits and coastal barriers embedded in shaley marine and lagoonal deposits. Palaeogeographically, deposition of the Rijnland Group occurred during large-scale transgression due to tectonic subsidence and global eustatic sea level rise (Haq, et al., 1987; NITG, 2002). This transgression caused sedimentary onlap on the flanks of the surrounding highs.

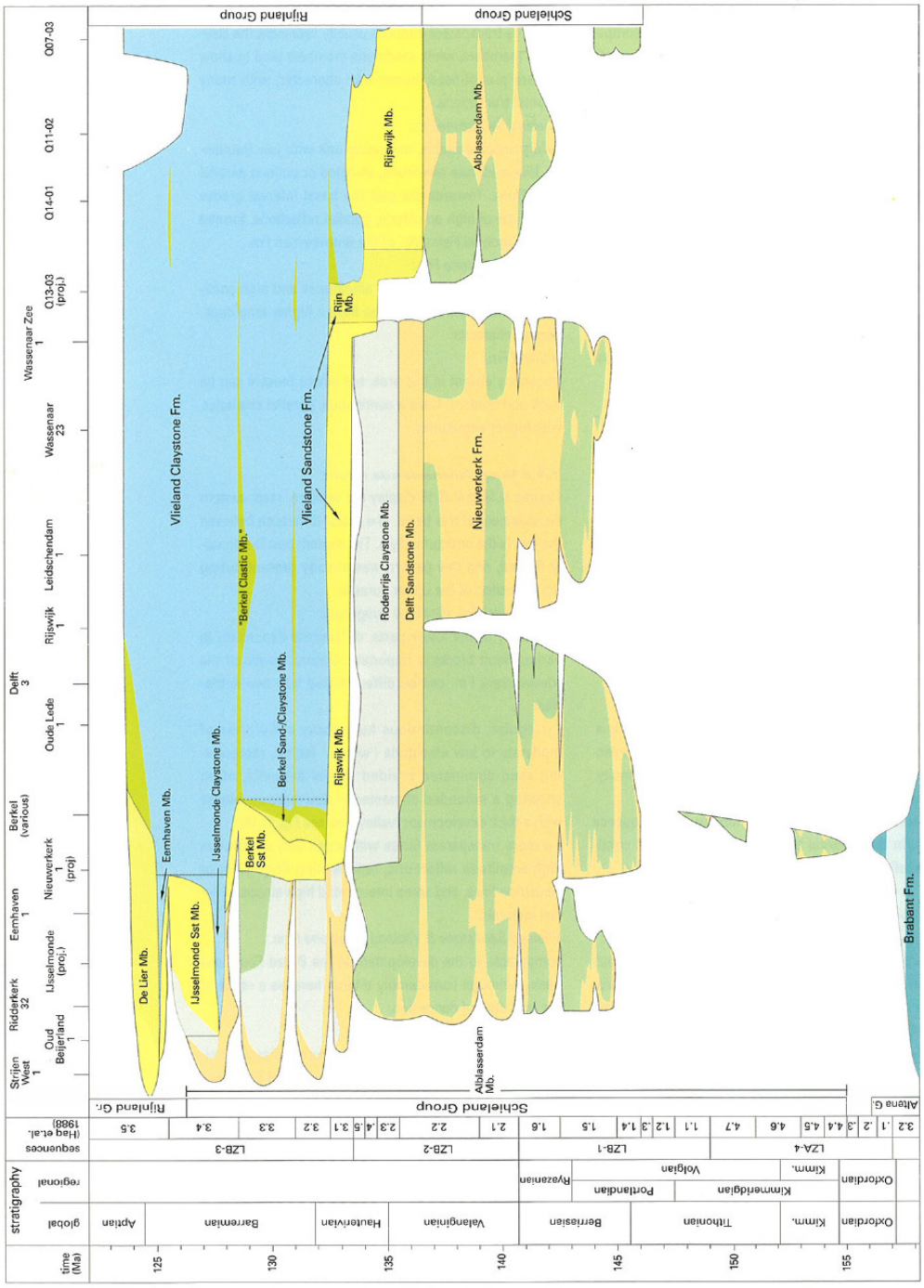

Figure 2. Late Jurassic-Early Cretaceous lithostratigraphic section (pre-Aptian) through the West Netherlands Basin (Van Adrichem Boogaert and Kouwe, 1993).

2 Methods

2.1 Dataset

This study exclusively utilizes public domain data (Table 1). The main 3D structural framework is derived from seismic horizons and faults mapped by TNO (Duin, et al., 2006). Aquifer thickness, lithofacies and petrophysical properties were obtained from (digital) well log data and core plug measurements.

The 3D structural framework covers an area of approximately 3000 km^2 (Fig. 1). The base and top of the model are defined by the base and top of the Rijnland Group. Both surfaces as well as the major faults were obtained by seismic interpretation of available 2D and 3D surveys in the regional mapping programme (scale 1:250,000) of TNO (Duin, et al., 2006).

A total of 538 wells were available for this study (Table 1, Appendix 1). Most of these wells have stratigraphic markers for the members in the Rijnland Group and well trajectory information. However, digital wireline logs (gamma ray, sonic, neutron, density) and core plug measurements (porosity and permeability) are available for a few wells only.

2.2 Well data processing

2.2.1 Lithofacies

In the absence of core descriptions for the wells, sand-shale intervals were interpreted using gamma gay (GR) logs. For 3D facies modelling, 77 unique wells containing GR were used. When composite well logs were absent, GR logs were manually selected and joined into single GR logs. Cluster analysis was used to analyse the added value of neutron, density and sonic logs to create a better separation of sand-shale intervals compared with GR logs alone (Appendix 2). Cluster analysis is an exploratory data analysis tool which aims at sorting objects into groups in a way that the degree of association between two objects is maximal if they belong to the same group and minimal otherwise. The analysis of wells from the study area indicated that the use of logs other than GR logs does not lead to a better separation of sand-shale intervals. Accordingly, the sand-shale intervals have been distinguished using GR logs only.

The measured (absolute) GR value ranges differ between wells, mainly because the used tools are specifically calibrated to each well. Consequently, the GR values corresponding with sand and shale differ between the wells. Therefore, a ratio of the minimum and maximum GR values has been used, to identify the extremes of GR for each lithology. The ratio was defined based on a comparison of GR and lithology as recorded in composite well logs. After clipping of the logs to the studied stratigraphic interval and removal of peaks (GR > 150), relatively low GR values were labelled as sand and high GR values as shale. The sand-shale division based on the GR logs (Fig. 3), resulted in three lithofacies: sand, clay and a waste class (sandy clay/clayey sand).

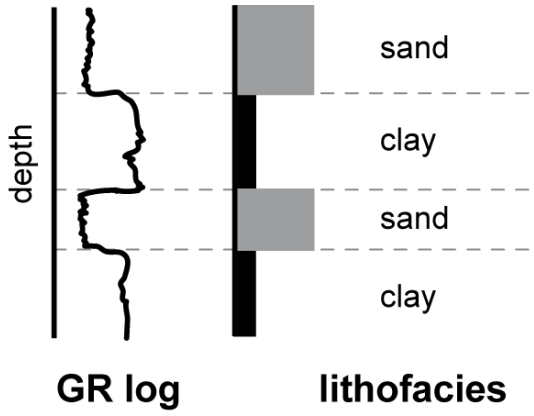

Figure 3. The creation of lithofacies using gamma ray logs and stratigraphic markers. In case a gamma ray log was absent, lithofacies were defined based on stratigraphy.

2.2.2 *Porosity logs*

Porosity logs for deposits within the Rijnland Group were calculated for 94 wells using bulk density (RHOB) and neutron (NPHI) logs, and core plug measurements (Fig. 4):

A. When only bulk density logs were available, porosity logs were calculated using grain density data from core plugs and fluid density (Fig. 4A). Fluid density was set at the average value between fresh and salt water (1.1 g/cm^3), without correction for hydrocarbons in the fluid;
B. Otherwise, neutron logs were used, with a correction (0.045) for the fact that neutron logs represent porosity based on carbonate rock (Fig. 4B)
C. If bulk density and neutron logs were available, both aforementioned methods were used and averaged (Fig. 4C).

When available, core plug measurements were used to correct the calculated porosity log towards the measured core plug porosity values.

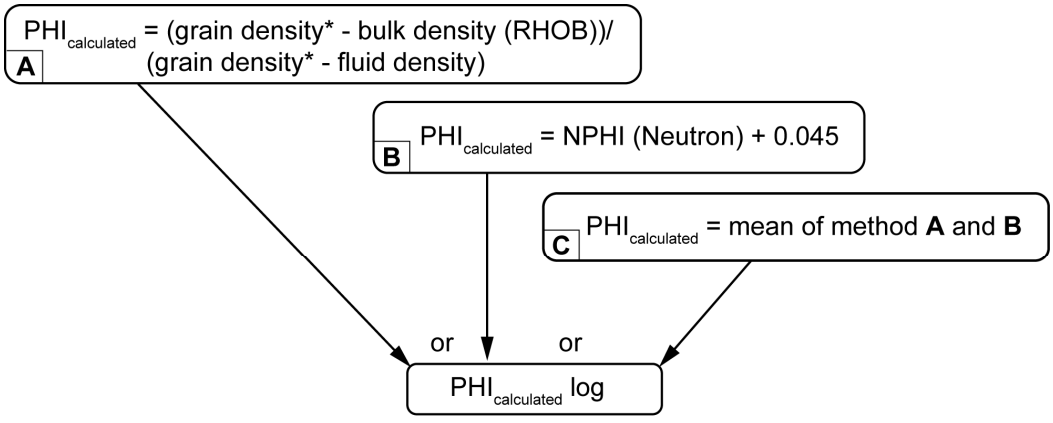

Figure 4. Calculation of porosity logs following method A, B or C, depending on data availability. The calculated porosity log was corrected to core plug porosity measurements when available.

Data type	**Available**	**Source**	**Application**
Well locations (oil and gas, including sidetracks)	538	DINO BRH	General overview, not all wells were used
Well deviations	496	DINO BRH	Building 3D model, not all wells were used
Well logs (GR, RHOB, NPHI)	GR=77, RHOB=50, NPHI=39	DINO BRH	Calculating properties for 3D model
Composite well logs	43		
Stratigraphic markers	510	DINO BRH	General overview, not all wells were used
Core plugs (PHI, K)	Poro-perm relationship=76	DINO BRH, (Duin et al. 2006)	Calculating properties for 3D model
Base CK+N, KN and S surfaces	n/a	(Duin et al. 2006)	Creating stratigraphic horizons
3D faults	n/a	(Duin et al. 2006)	Constructing fault model and 3D pillar grid
3D seismic surveys:	n/a	DINO NLOG	Reconstructing palaeo topography and sedimentary basin fill configuration
Biesbosch_L3NAM1986A			
DenHaag_L3NAM1991A			
Dordrecht_Noord_L3NAM1988H			
Dordrecht_Zuid_L3NAM1988J			
Gouda_Noordoost_L3NAM1989B			
Gouda_Zuidwest_L3NAM1989A			
Haastrecht_L3NAM1988G			
Leiden_Pijnacker_Gouda_L3NAM1989K			
Leiden_Pijnacker_L3NAM1989J			
Monster_L3NAM1990C			
Mookhoek_L3NAM1991B			
Pijnacker_dll_L3NAM1985P			
Pijnacker_L3NAM1985R			
Waalhaven_L3NAM1985A			

Table 1. Data used for modelling. See Appendix 1 for well names. DINO BRH = TNO DINO borehole table.

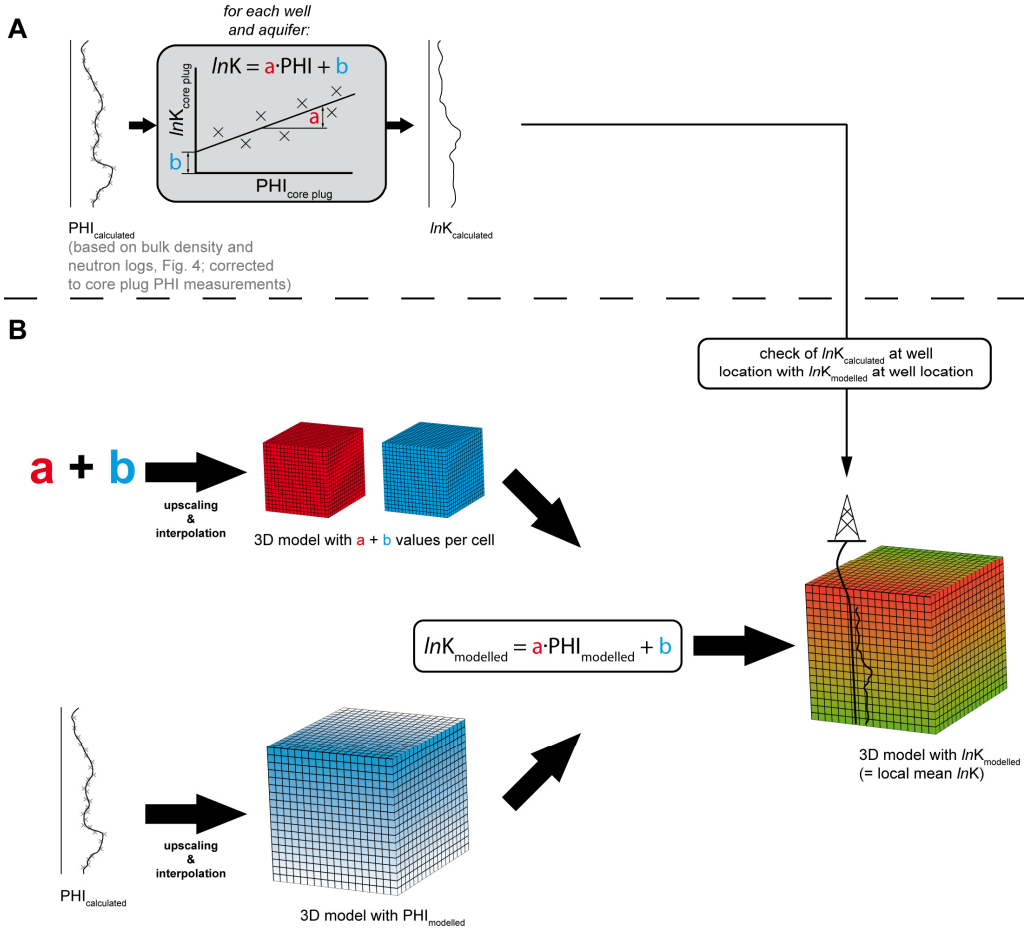

Figure 5. Permeability calculations: (A) calculated porosity ($PHI_{calculated}$) logs which are corrected to core plug measurements, are used to calculate permeability logs ($lnK_{modelled}$). The linear core plug *ln*K-PHI relationship was used to convert porosity to permeability for each well with core plug measurements; (B) the parameters of the linear core plug *ln*K-PHI relationship is used to calculate the 3D *ln*K model. Inputs for this formula are values from 3D models of a, b and $PHI_{calculated}$ values.

2.2.3 *Permeability logs*

Permeability logs were calculated using the linear relationship between porosity (PHI) and the natural logarithm of permeability (*ln*K). This relationship was calculated for each well containing core plug measurements (Fig. 5A). The slope (**a**) and intercept (**b**) of this relationship were used to calculate permeability logs from porosity logs, but only when core plug measurements were available for the well, otherwise no linear relationship could be constructed. The calculated permeability log ($lnK_{calculated}$) was used later in the modelling workflow to adjust permeability values in the 3D model at well locations (Fig. 5B & 15).

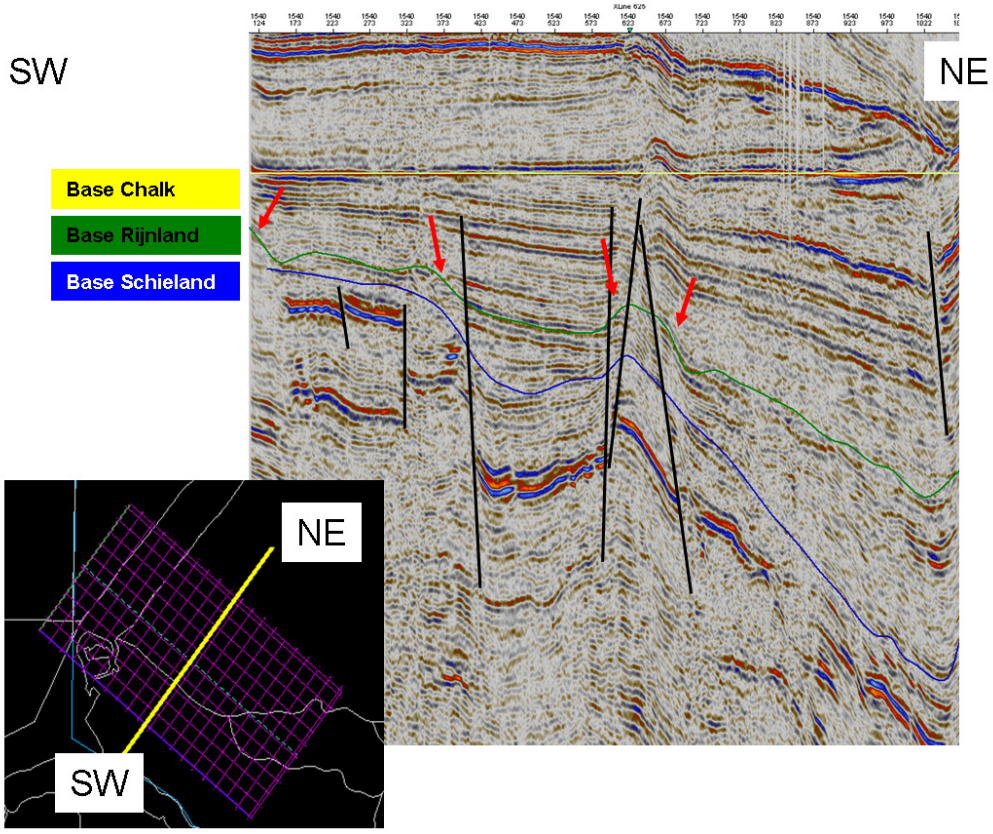

Figure 6. Seismic section through the West Netherlands Basin, showing onlapping strata (red arrows) in 3D seismic survey L3NAM1990C.

2.3 Modelling assumptions

2.3.1 Sedimentary architecture

Based on seismic sections across the study area, flattened on the top of the Rijnland Group, the sedimentary architecture of the WNB has been established.

Seismic sections clearly show the dominant occurrence of strata onlapping the basin margins, which is for example evident in seismic sections flattened on the top of the Rijnland Group (Fig. 6). This is supported by the assumed tectonic history of the area, where base-level rise and syn-sedimentary subsidence occurred simultaneously during deposition of the Rijnland Group (Den Hartog Jager, 1996). The onlapping of layers has been accounted for in the 3D model (grid cells parallel to top Rijnland Group surface). Although minor deviations from the onlap model are present in the WNB sedimentary fill, the onlap configuration is assumed to be well suited for the regional scale of this study.

2.3.2 Chronology

The contact between the continental Schieland Group and the marine Rijnland Group is diachronous as a result of the transgressive character of the sedimentary sequence (Fig. 7). To differentiate between the different members in the Rijnland Group and to be able to map these members using seismic surveys, time lines based on absolute chronology

are desirable. However, both detailed seismic mapping and detailed absolute chronology for the sandstone members in the Rijnland Group are not available. Therefore, the distribution of sandstone is modelled stochastically, without making a distinction between the different sandstone members.

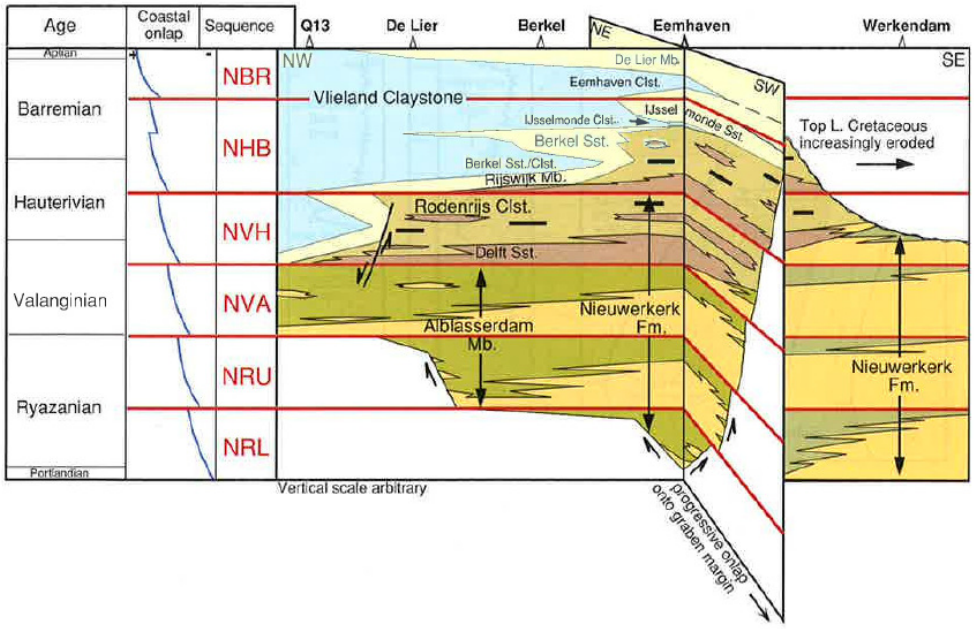

Figure 7. Schematic cross sections through the West Netherlands Basin with sequence stratigraphic interpretations. Sequence names: NRL = Neocomian/Ryazanian Lower, NRU = Neocomian/Ryazanian Upper, NVA = Neocomian/Valanginian, NVH = Neocomian/Valanginian - Hauterivian, NHB = Neocomian/Hauterivian - Barremian, NBR = Neocomianl Barremian (Den Hartog Jager, 1996). See Fig. 2 for chronostratigraphy.

2.3.3 *Porosity-permeability relationships*

Although the relationship between porosity and permeability is known to be highly variable, the dataset used here suggests at least a reasonable relationship between porosity and permeability from core plug measurements in single wells (Fig. 8). This is true especially when compared with the use of one single relationship for the entire Rijnland Group interval. No significant relationship has been found between burial depth and permeability for sands of the Rijnland Group in the WNB (Fig. 9). Explanations for this may be (1) a limited depth of burial and thus limited diagenesis; (2) an absent correlation between diagenesis and present-day depth due to inversion; (3) permeability differences within the sandstones due to sedimentary facies differences; (4) different diagenesis along the large number of faults in the WNB due to fluid flow. Because of the apparent absence of a relationship between burial depth and permeability, no measures were taken to correct permeability based on burial depth.

The linear porosity-permeability relationship for each well and aquifer (**a** + **b**) was upscaled and interpolated throughout the entire 3D model space (Fig. 5B). As **a** and **b** are correlated (Fig. 5A), collocated co-kriging is applied for interpolation (i.e. parameter **b** is interpolated first and is used as a co-variable for the kriging of **a**). Based on this relationship and the 3D porosity model, the 3D distribution of the permeability ($ln K_{modelled}$) has been established (Fig. 5B).

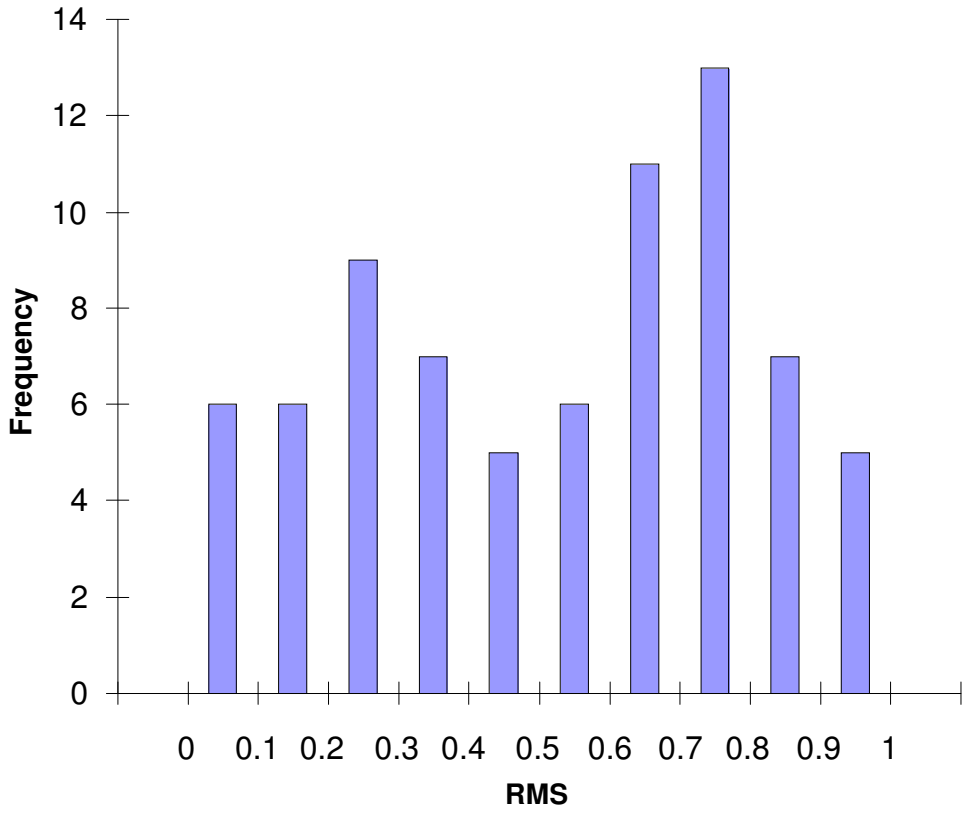

Figure 8. Root mean square (RMS) error of the relationship between porosity (PHI) and permeability (*ln*K) from core plug measurements for individual wells (n=76) per aquifer. Although a part of the relationships has low RMS values, a large amount has a good RMS above 0.6.

2.4 Modelling workflow

The 3D modelling of the lithofacies and properties (porosity and permeability) was subdivided into three major phases:

1. Construction of a 3D grid model consistent with the seismic horizon interpretations and stratigraphic marker depths in the wells;
2. Population of the 3D grid cells in the model with sand and shale lithofacies;
3. Assignment of porosity and permeability values to the sand lithofacies in the model.

Most of the modelling (i.e. the construction of the 3D grid model and the population and assignment of lithofacies and properties) was performed using Schlumberger Petrel 2009 software. Geovariances Isatis software was used for exploratory data analysis and variogram modelling.

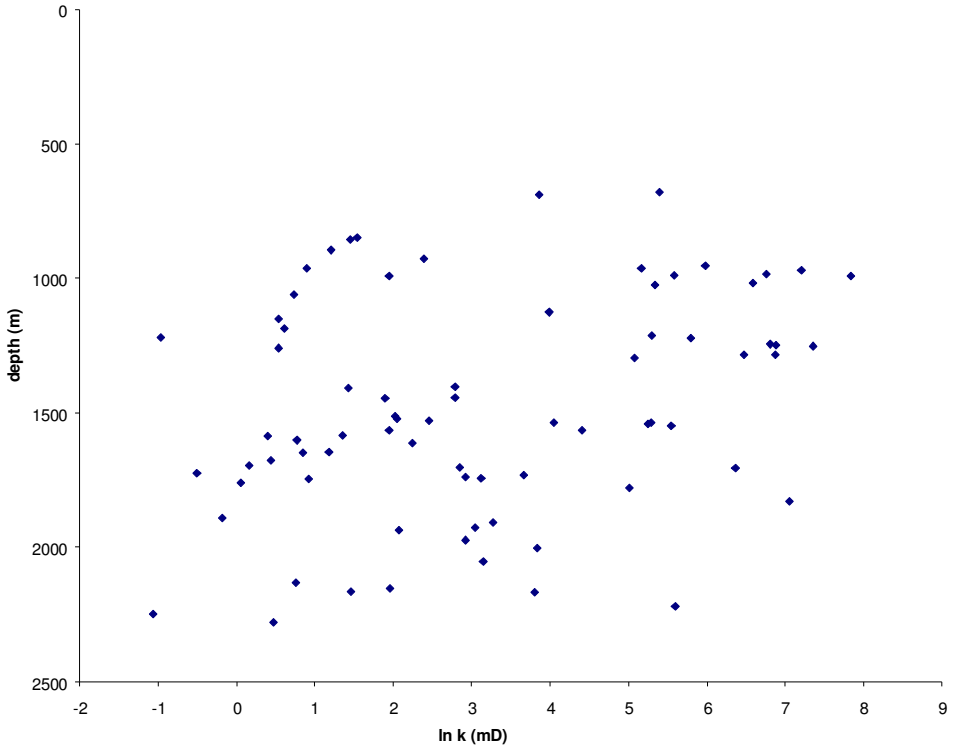

Figure 9. Sample depth versus lnK for core plug permeability of wells in the Rijnland Group of the West Netherlands Basin; no relationship between burial depth and permeability can be observed.

2.4.1 *3D grid model*

The 3D grid model (cell-size 250 x 250 m) forms the structural basis for the lithofacies model and was constructed from the major regionally mapped faults and the top and basal surfaces of the Rijnland Group (Fig. 10). Both surfaces were calibrated to the stratigraphic marker depths in the wells by interpolating and subsequently adding the mis-tie distance. The model was vertically regularized into five meter thick layers which approximate the observed onlapping relationship (§ 2.3.1).

2.4.2 *Upscaling*

Well data (lithofacies, $PHI_{calculated}$, $lnK_{calculated}$, and linear porosity-permeability relationship parameters **a** + **b**) were upscaled to the 3D grid cells. The lithofacies data comprise discrete values. Cells penetrated by multiple wells or wells that contain more than one lithofacies code were set to the lithofacies that occurs most frequently within the cell. The porosity logs were upscaled by calculating the arithmetic mean of all logs penetrating the cells. To account for the wide distribution of $lnK_{core\ plug}$ values, $lnK_{calculated}$ values at the well locations were upscaled from the wells and used during modelling (§ 2.4.5).

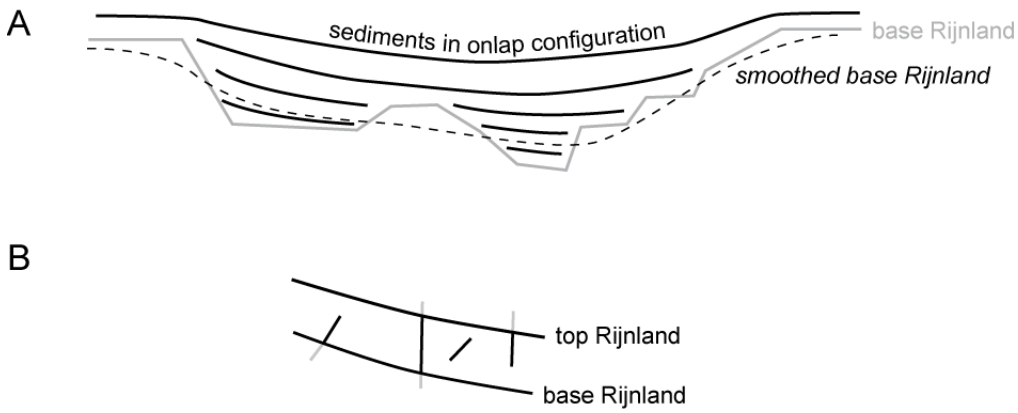

Figure 10. 3D model: (A) use of smoothed base-Rijnland Group surface to generate sedimentary onlap configuration; (B) faults included in Rijnland Group interval 3D model.

2.4.3 Lithofacies modelling

The lithofacies modelling workflow (Fig. 11) uses the upscaled lithofacies from the wells to populate the entire 3D grid model. For this study the Sequential Indicator Simulation (SIS) algorithm was used for interpolating the discrete lithofacies values to the grid cells that are not penetrated by well logs. The SIS algorithm builds multiple random realisations of the 3D facies distribution, each of which honours the upscaled data and resembles the target distribution provided. Although the outcome of each realisation is different from the other, they are all equally probable. The SIS realisations represent the expected heterogeneity of the lithofacies distribution in the Rijnland Group through the use of variograms. The variograms for the Rijnland Group (Fig. 12) describe the spatial continuity in horizontal and vertical directions as determined from the upscaled lithofacies data. Besides the variograms, a target distribution of 65 % sand and 35 % shale has been applied, which represents the average sand-shale distribution observed in the well data. This may result in an over-estimation of the sand fraction because most wells have targeted sand lithofacies. However, since other options were limited within the framework of this study and because the model honours well data, the lithofacies modelling has resulted in a relatively reliable lithofacies distribution.

The expected net sand distribution maps (i.e. the total sand thickness in the entire Rijnland Group) were determined based on the 50 lithofacies realisations (Maps 1A-D).

2.4.4 Porosity modelling

The porosity modelling workflow (Fig. 13) assigns porosity values to the modelled sand lithofacies in the Rijnland Group. Sequential Gaussian Simulation (SGS) was used to interpolate the upscaled log ($PHI_{calculated}$) values from the wells throughout the model. Like the SIS algorithm, the SGS algorithm builds multiple random realisations that both honour the upscaled values and represent the expected target distribution and heterogeneity. The SGS algorithm is intended for interpolating continuous variables which are assumed to have values with a more or less normal (Gaussian) distribution. The SGS algorithm in the Petrel software therefore applies a normal score transformation on the absolute property values before interpolation (i.e. transforms the data set such that the variable has a normal Gaussian distribution with a mean of zero

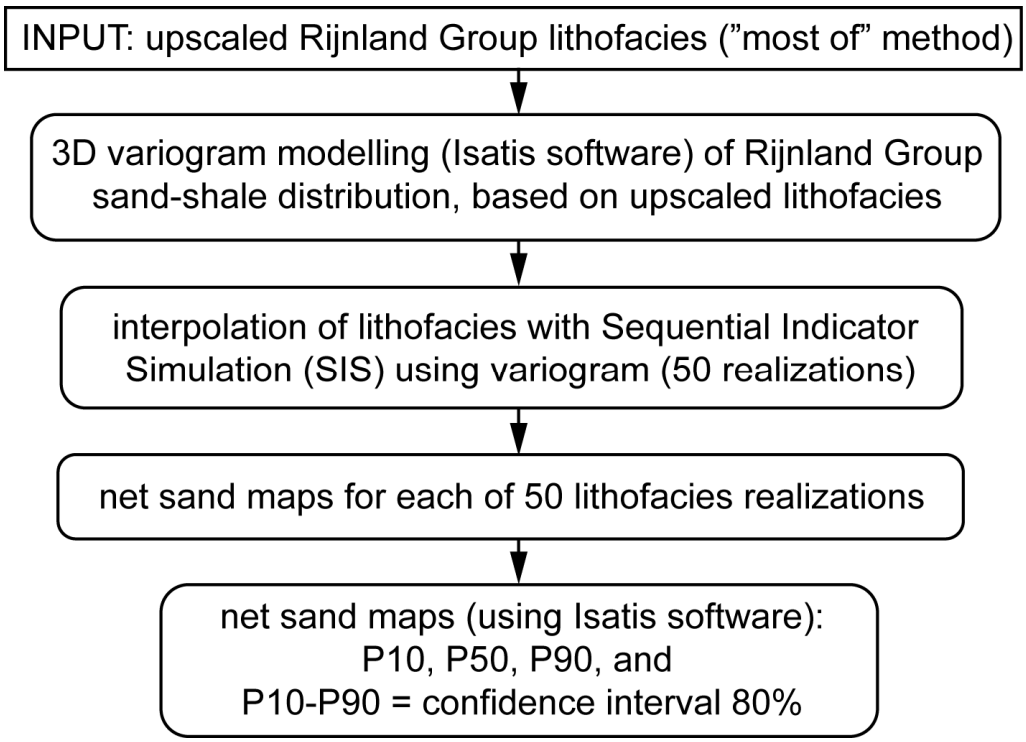

Figure 11. Workflow used for facies modelling. See paragraph 2.4.3 for explanation.

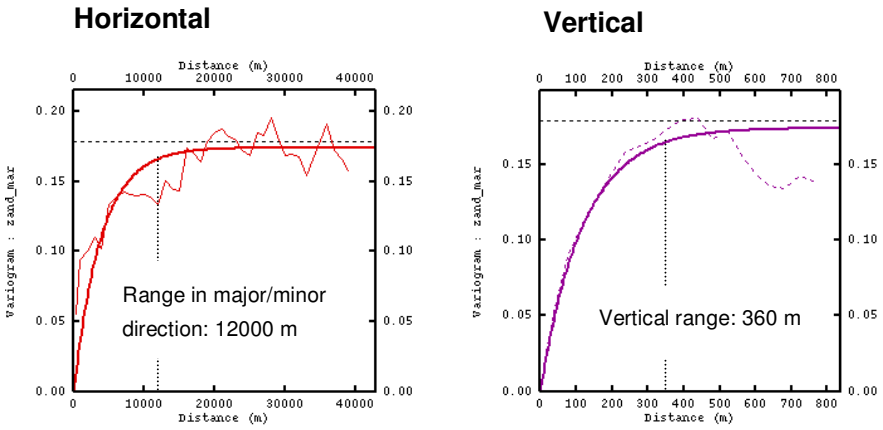

Figure 12. Horizontal and vertical variogram for sand lithofacies in the Rijnland Group.

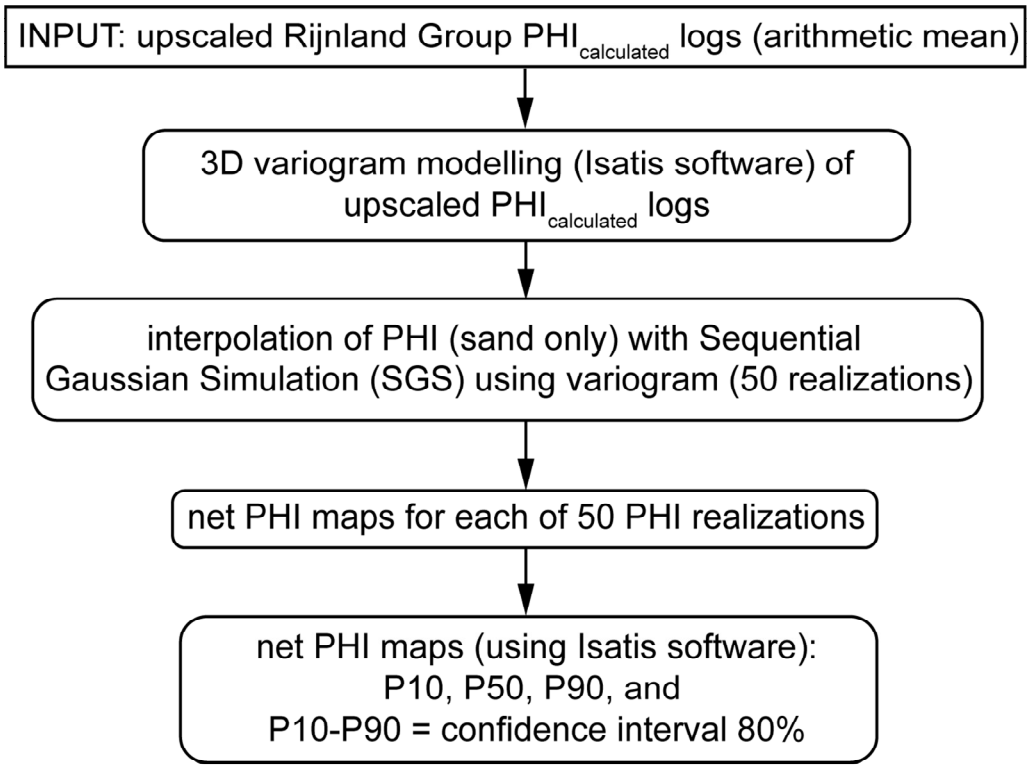

Figure 13. Workflow used for porosity modelling. See paragraph 2.4.4 for explanation.

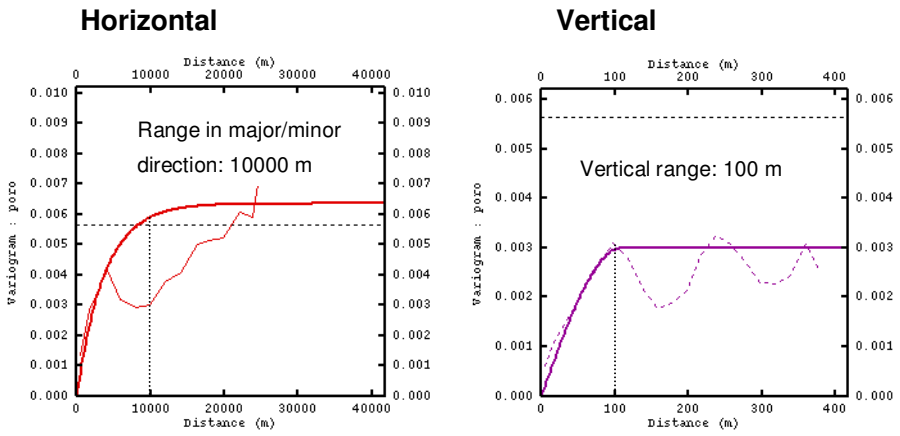

Figure 14. Horizontal and vertical variogram for porosity in the Rijnland Group.

and a standard deviation of one). The interpolated values are finally back-transformed to absolute values. The horizontal variogram for upscaled porosity values is quite robust (Fig. 14). However, the vertical variogram does not indicate a very clear correlation of the available data.

In total 50 random porosity realisations were obtained (one for each lithofacies realisation). Only the porosity distribution in the cells with a sand lithofacies was considered. From these 50 realisations, net porosity maps were obtained (Maps 2A-D).

2.4.5 *Permeability modelling*

As discussed above (§ 2.3.3), permeability is correlated with porosity (Fig. 5A) through the following relationship obtained from linear regression of core plug measurements:

$$ln\mathrm{K}_{\mathrm{modelled}} = \mathbf{a} \cdot \mathrm{PHI}_{\mathrm{modelled}} + \mathbf{b} \quad \text{(equation 1)}$$

where $ln\mathrm{K}_{\mathrm{modelled}}$ is the natural logarithm of permeability, $\mathrm{PHI}_{\mathrm{modelled}}$ is the porosity and **a** and **b** are the linear regression coefficients. The coefficients of this linear correlation are determined per well and per aquifer, resulting in one set of **a** and **b** per well and aquifer. Using these coefficients, $ln\mathrm{K}_{\mathrm{modelled}}$ values are determined based on each of the 50 porosity realisations.

Because the $ln\mathrm{K}_{\mathrm{modelled}}$ values are obtained from the porosity-permeability relationship in equation 1, they do not correctly represent the wide permeability distribution representing the variability of permeability in the aquifers. This is illustrated in the scattered point cloud of $\mathrm{PHI}_{\mathrm{core\ plug}}$ versus $ln\mathrm{K}_{\mathrm{core\ plug}}$ (Fig. 15, scatter plot). Linear regression only provides the best (average) linear fit through the point cloud. If a porosity value is transformed through this relationship, it will thus result in an *average* *ln*K value or in modelling terms, a local mean. In reality each porosity value corresponds with a range of possible *ln*K values (Fig. 15).

In order to correctly represent the trend of the porosity-permeability relationship as well as the wide permeability distribution, an additional modelling step is required. For this step, the local mean $ln\mathrm{K}_{\mathrm{modelled}}$ values were used as a locally varying mean trend-variable for interpolation of $ln\mathrm{K}_{\mathrm{calculated}}$ using the Sequential Gaussian Simulation (SGS) algorithm. Using this algorithm, the upscaled $ln\mathrm{K}_{\mathrm{calculated}}$ values (Fig. 5A) were upscaled and interpolated to create a 3D model with $ln\mathrm{K}_{\mathrm{corrected}}$. The variability and spatial correlation of the upscaled $ln\mathrm{K}_{\mathrm{calculated}}$ variable are captured in the modelled variograms (Fig. 16). Due to the relatively low data density and heterogenic nature of the upscaled $ln\mathrm{K}_{\mathrm{calculated}}$ values, the variograms are not as robust as they appear for the lithofacies and porosity variables.

For each local mean $ln\mathrm{K}_{\mathrm{modelled}}$ realisation, one interpolated $ln\mathrm{K}_{\mathrm{corrected}}$ realisation was calculated, resulting in a total of 50 $ln\mathrm{K}_{\mathrm{corrected}}$ realisations (Fig. 15). Each of these realisations correctly represents the variability defined by the variogram.

The last step involved multiplication of the exponent of each $ln\mathrm{K}_{\mathrm{corrected}}$ distribution by cell thickness (of sand lithofacies cells) and vertically summing of these values in order to obtain 50 realized maps of the total transmissivity of the Rijnland Group interval. From these 50 realisations, net transmissivity maps were derived (Maps 3A-D).

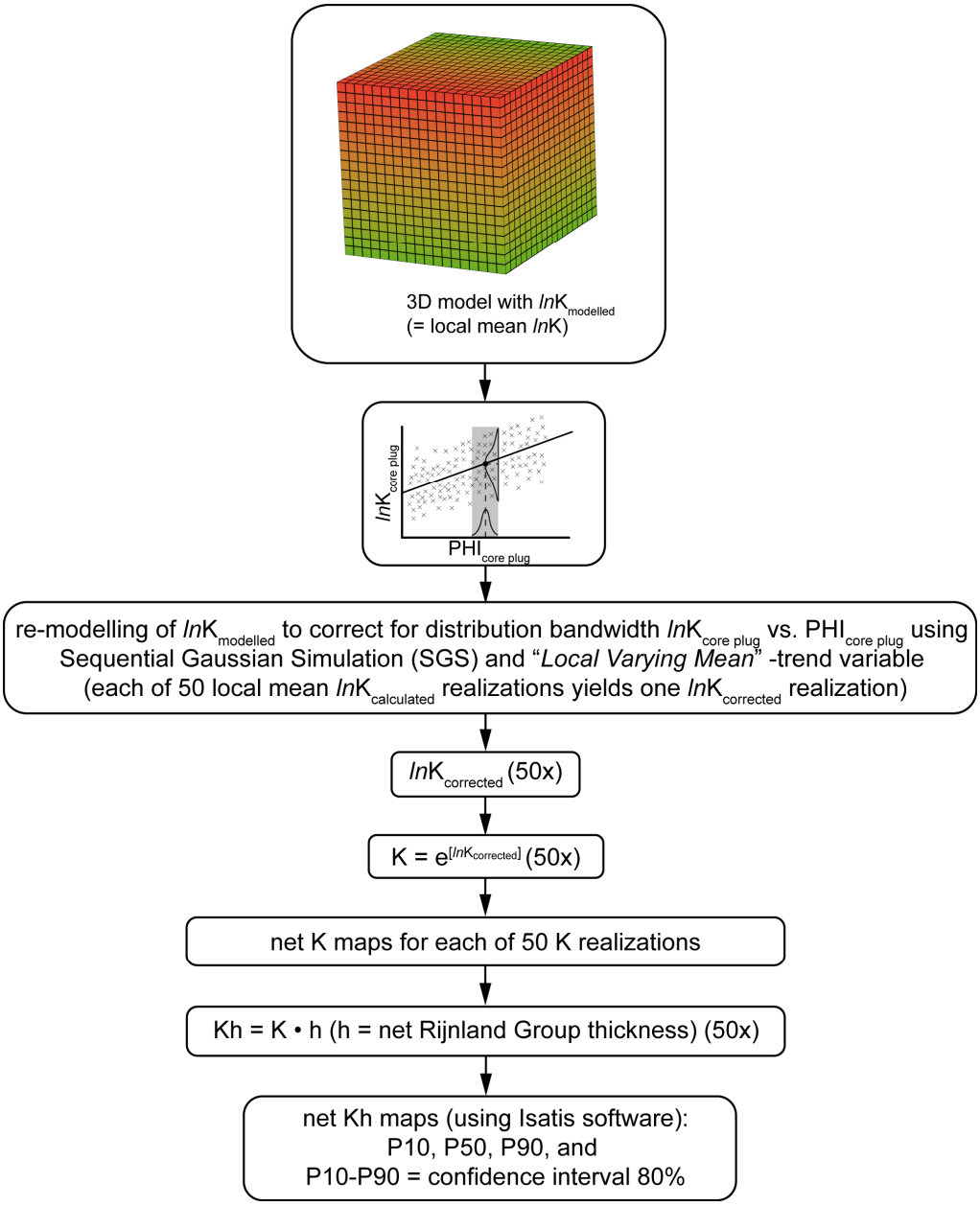

Figure 15. Workflow used for permeability modelling. See paragraph 2.4.5 for explanation.

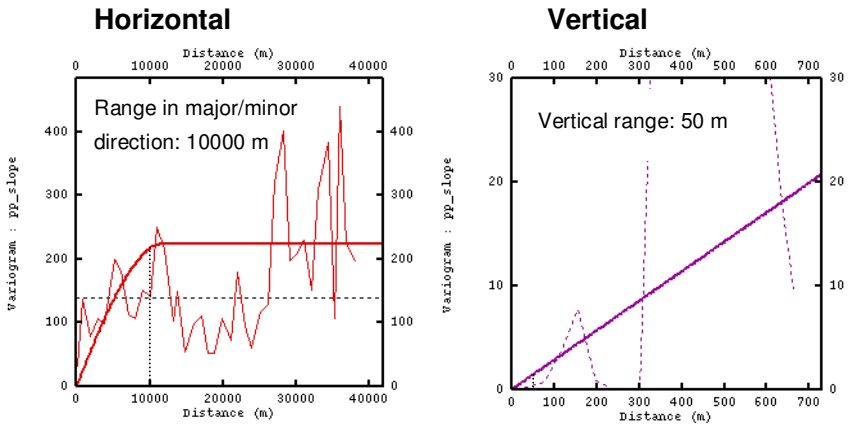

Figure 16. Horizontal and vertical variogram for intercept (b) in the Rijnland Group.

3 Results and discussion

3.1 3D models

The models created for the Rijnland Group in the West Netherlands Basin incorporate possible realisations of the spatial distributions of lithofacies, porosity and permeability based on the known information at well locations. The "unknown" model space is populated using stochastic estimation algorithms as described in Chapter 2.

A total of 50 random realisations have been calculated for the facies, porosity and permeability distributions. These distributions are considered equally probable and aim to represent the heterogeneity of the property distributions in the Rijnland Group conform the data characteristics and geological concepts.

Depending on the degree of spatial correlation (which is defined by the variograms), individual realisations are more or less similar close to wells, while further away from the wells, the variability among realisations increases. Maps 1B, 2B and 3B present the P50 (50% chance that the actual value is either higher or lower than the value presented in the map). The uncertainty ranges are defined by the P90 (90% chance that the actual value is equal to or higher than the map value) and P10 (10% chance that the value is equal to or higher than the map value) maps. In other words, the chance that the true value lays within the P10-P90 range equals 80%.

3.1.1 Lithofacies model and net sand maps

The overall lithofacies distribution in the 3D lithofacies model is more or less consistent with the geological concepts and available well data. Sand layers in the model correspond with the Rijn, Rijswijk, Berkel Sandstone, IJsselmonde Sandstone and De Lier Members. According to well data, these members are laterally continuous over distances ranging between 20 and 30 km. Typical measured thicknesses in the wells range between 5 and 280 meters. These layers appear at correlatable stratigraphic levels in most wells and are generally well connected by the interpolation algorithm and applied variograms. The 3D model contains sand layers with lateral and vertical dimensions comparable to those obtained from well data (Fig. 17). Besides the continuous sand layers, many thin sand bodies with a patchy distribution are present throughout the entire model. These sand bodies also appear in the wells as local uncorrelated features (Fig. 18A).

In some realisations stacked individual layers may appear as one connected sand body resulting in a local abnormally thick sand occurrence (Fig. 18B). These stacked occurrences are considered to be the result of the interpolation algorithms and settings. In areas with a low well density, the model may result in a stacking of clay or sand sediments, while still honouring well data and input settings (35 % sand – 65 % shale).

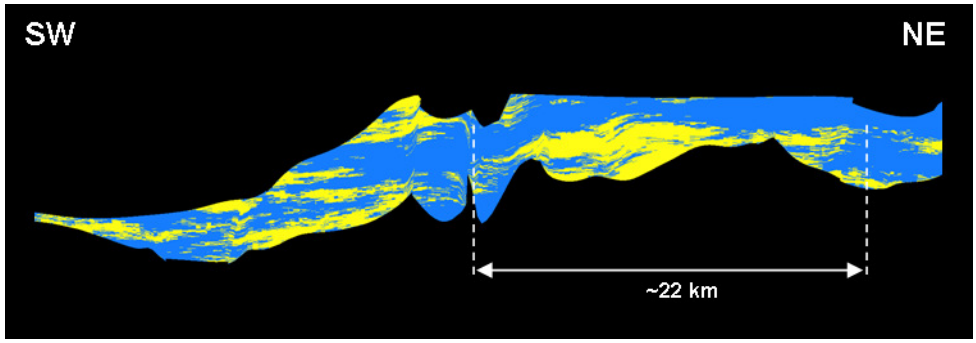

Figure 17. An example of sand-layer dimension in an arbitrary cross section through a random lithofacies realisation.

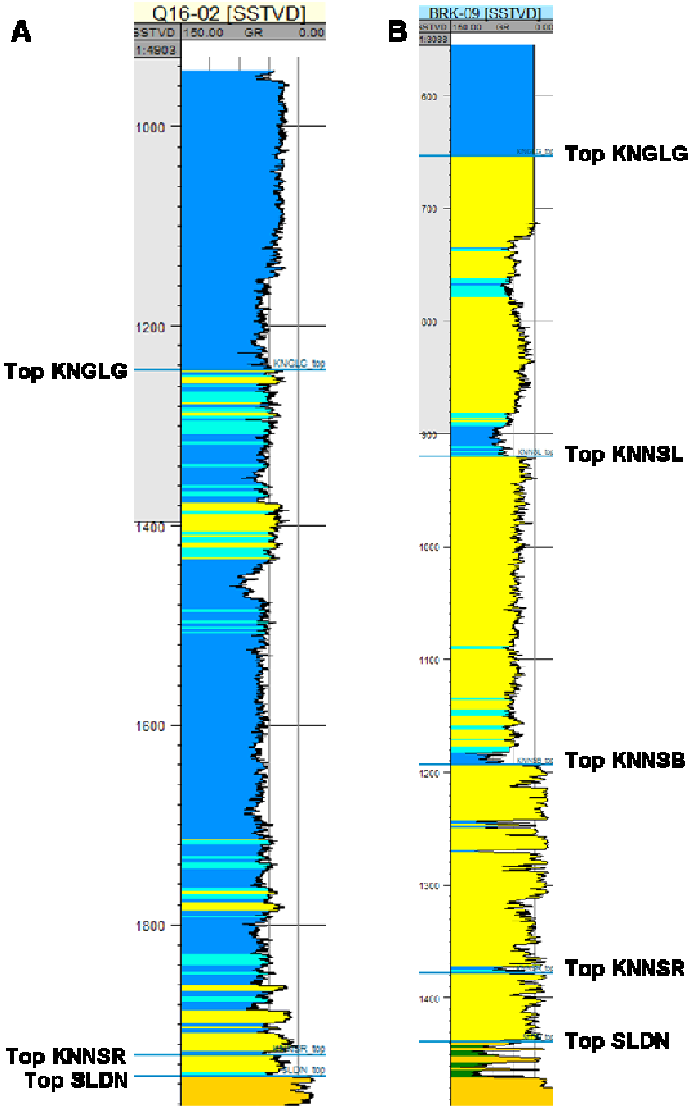

Figure 18. Gamma ray logs representing shale and sand dominated lithofacies: (A) shale dominated log with thin intercalated sand layers; (B) sand dominated log with only thin shale intervals, representing stacked sand bodies.

These anomalies have little influence on the net sand maps because they are outliers which are compensated for by averaging using the other realisations. Besides the lateral extent and thickness, the onlap configuration is apparent in most realisations, agreeing with data-based observations (Fig. 19).

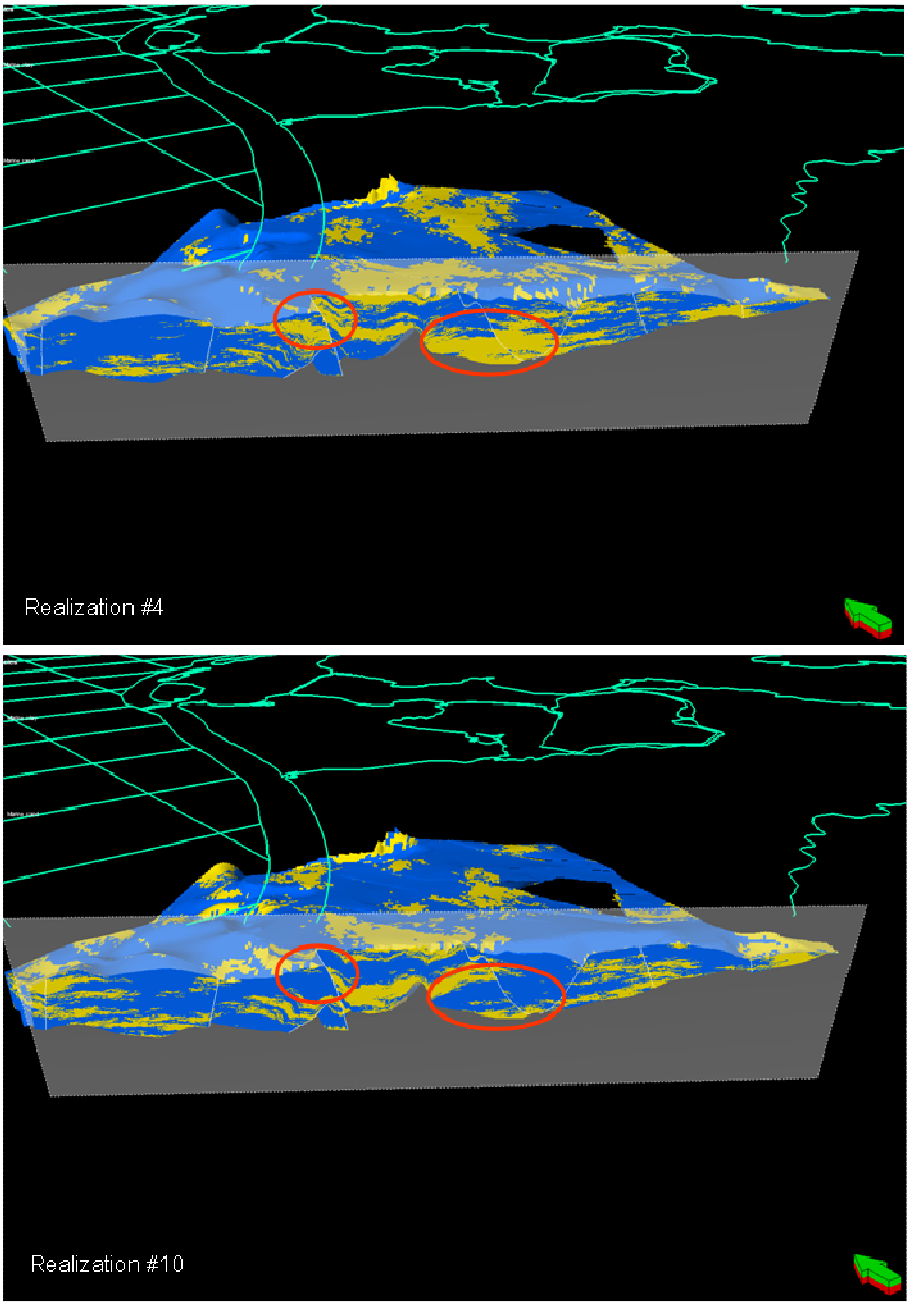

Figure 19. Two realisations of modelled sand distributions (yellow) showing two extreme outcomes based on the same variogram settings. The differences (red circles) clearly demonstrate that the model realisations reflect possible sand-shale distributions.

The net lithofacies map (Map 1B) shows the P50 of the net sand thickness, the distribution of which is strongly related with the total thickness of the Rijnland Group. The values in this map reach over 500 m of thickness in the central part of the WNB, while especially along the basin margins sand may be entirely absent.

The P10-P90 map (Map 1D) represents the range that includes 80% of the modelled thickness values. Smaller values indicate a narrower range and thus a lower uncertainty. Smallest differences are typically present along the basin edges and at well locations. The areas with the thickest onshore sand occurrences northwest and south of Den Haag and north of Rotterdam (Map 1B), have the highest uncertainty (Map 1D). These areas are located in grabens where the thickest accumulations within the Rijnland Group occur. However, these areas are characterized by the lowest well densities, hence the high uncertainty here. Remarkably, the small area with a large sand thickness (P50 > 500 m) south of Den Haag also has a relatively low uncertainty (P10-P90 = 50-200 m) when compared with other areas with a large sand thickness.

3.1.2 Porosity model and net porosity maps

The modelling of porosity in the 3D porosity model was limited to the sand lithofacies. Therefore, the porosity patterns follow the lithofacies distribution. Within the sand lithofacies, porosity trends cannot be discerned based on the 50 realisations. Porosity values in the 3D model generally follow a normal distribution with an average of 0.21 ± 0.06 (1σ), which is virtually equal to the well logs.

The net porosity map (Map 2B) with the P50 values visualizes areas where the chance of either higher or lower porosities than indicated is 50%. The values in the mean net porosity map range between 0 and > 0.27 (fraction). The central part of the WNB (generally between Den Haag, Rotterdam and Gouda) is characterized by the occurrence of the highest porosity values. It must be stressed here that these values represent the complete Rijnland Group and not individual members or sand layers. Remarkably, the area west of Rotterdam and southwest of Den Haag contains lower porosity values, although some thick sand occurrences have been modelled here (Map 1B). Apparently the average porosity is lower in that area, leading to lower values in the net map than further to the northwest.

Where the net sand thickness is low, unreliable estimates of the average porosity may occur. This is because there are a limited number of sand-cells upon which the average porosity is based.

Map 2D shows the P10-P90 map with the 80% confidence interval. The smaller the value on this map, the less uncertainty there is at that location. The uncertainty appears to be low in a large part of the WNB. When comparing Map 2D with the Map 2B, it can be seen that although the uncertainty may seem relatively limited, it can still reach up to ~50% of the modelled value.

3.1.3 Permeability model and net transmissivity maps

The 3D permeability modelling is based on the 3D porosity models. Permeability modelling was only performed within modelled sand lithofacies occurrences. When examining the 50 permeability realisations, no clear trend can be observed. However, it can tentatively be stated that the lowest permeability values occur in sand layers at the base of the model, which may correspond with shaley intervals in the Rijswijk or Rijn

Members. The permeability ($lnK_{corrected}$) values in the 3D model range between -2 (~0.14 mD) and 9 (~8000 mD), which corresponds well with the value ranges of the input data. Comparison of $lnK_{modelled}$ with upscaled $lnK_{calculated}$ values (Fig. 20), indicates that there is virtually no difference between the two at the well locations. This confirms the robustness of the used methodology.

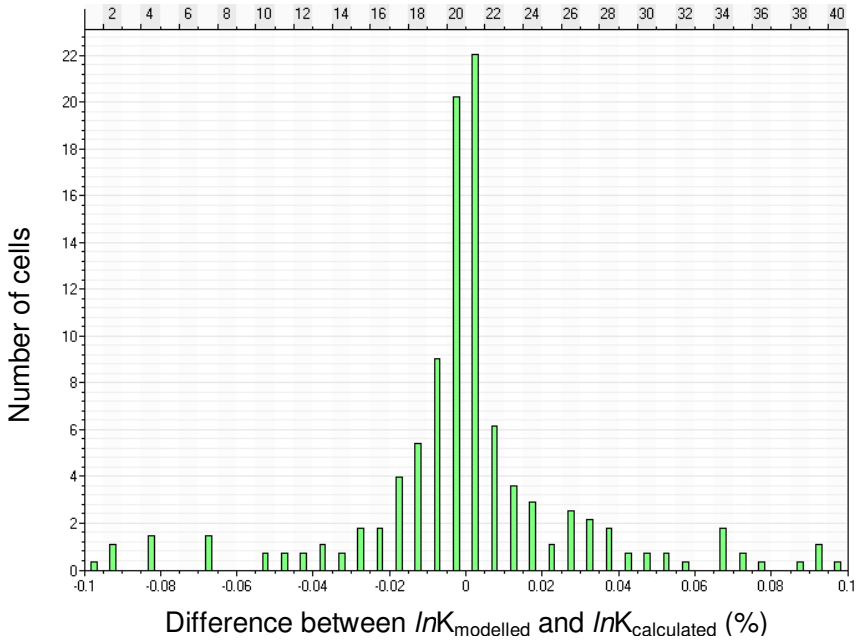

Figure 20. Difference between $lnK_{modelled}$ values and $lnK_{calculated}$ values at well locations. The diagram shows that nearly 60% of modelled values is equal to calculated values, and ~25% of modelled values in the wells differs only 0.1 *ln*K values. This implies that the used model is robust, at least at the well sites.

Based on the 50 permeability realisations, net transmissivity maps were calculated (Maps 3A-D). The net transmissivity P50 map (Map 3B), visualizes areas where the chance of either higher or lower transmissivities than indicated is 50%. Transmissivities vary between 0 and more than 750Dm. The highest transmissivities when penetrating the entire onshore Rijnland Group are expected in the central part of the WNB between Den Haag, Rotterdam and Gouda. This region corresponds with the area with the thickest onshore sand occurrences (Map 1B).

The P10-P90 map, results in a map with the 80% confidence interval (Map 3D). The area with highest uncertainties corresponds with the area with largest transmissivity values. Due to the naturally skewed distribution of permeability values, the P90 map (Map 3A) has lower values than the P50 map (Map 3B), which has much lower values than the P10 map (Map 3C).

The uncertainty in the net transmissivity map (Map 3D) is the result of a number of factors. The uncertainty of the modelled presence of sand is governed by the limited amount of data in the study area. Most wells are located in clusters on horst structures, and only a few wells are located in the areas in between. However, because the deposits of the members in the Rijnland Group consist of laterally widely extending but narrow

coastal and marine sands (Racero-Baena and Drake, 1996), their correlation across the study area using variograms ensures relatively robust 3D modelling. Nonetheless, there is a possibility of under or overestimating the sand thickness in especially the areas without well control.

The calculation of permeability values for the transmissivity maps depends on the modelled porosity, based on 94 wells with logs. These logs are also clustered in horst structures. The modelled porosity values are translated into permeability values, involving generalization of the detailed porosity-permeability measurements. This generalization cannot be avoided when performing 3D modelling.

3.2 Geological insights

Besides a 3D lithofacies model, and porosity and transmissivity maps of the Rijnland Group in the WNB, this study also resulted in new views of the geological development of the basin. Using 3D seismic surfaces (Duin, et al., 2006) and the technique of flattening on the top of the Rijnland Group, the palaeotopography at the start of deposition of the Rijnland Group was reconstructed.

The palaeotopography (Fig. 21) is relatively flat, most likely as a result of infilling of the basin by continental deposits of the Schieland Group and decreased tectonic subsidence around the Early Cretaceous (Den Hartog Jager, 1996). This relatively flat morphology implies that the transgressive system that progressively drowned the basin was not hindered by large topographic obstacles. The facies distribution was therefore most likely controlled by the interaction of sea-level rise and sediment supply.

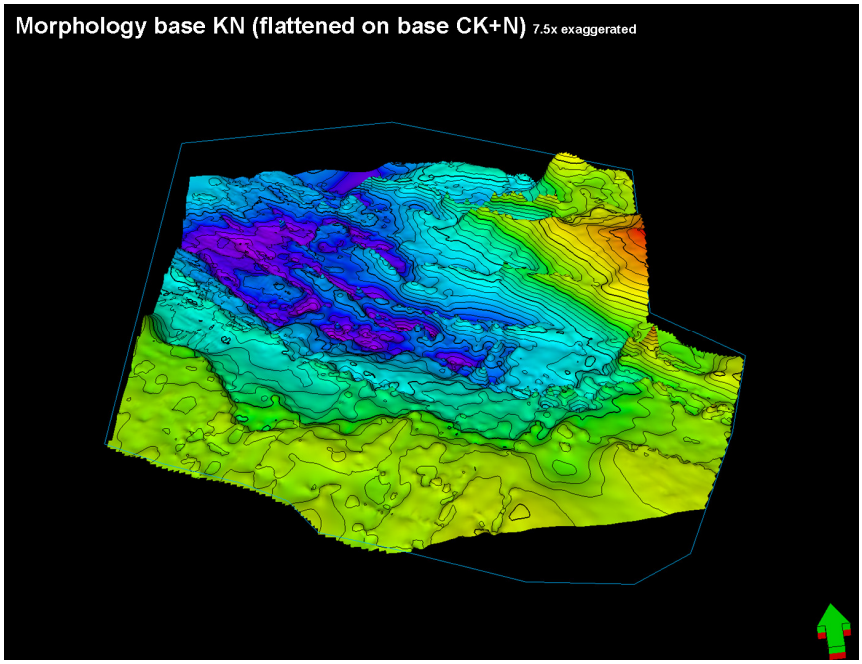

Figure 21. Palaeotopography at the base of the Rijnland Group, created by flattening of the mapped surface of the top of the Rijnland Group. Note the relatively flat morphology. Blue is low, red is high (original in time domain).

A clear landward stepping of marine environments can be identified when looking at the distribution of oil and gas fields, and wells in which the Rijn, Rijswijk, Berkel Sandstone, IJsselmonde Sandstone and De Lier Members have been encountered (Fig. 22).

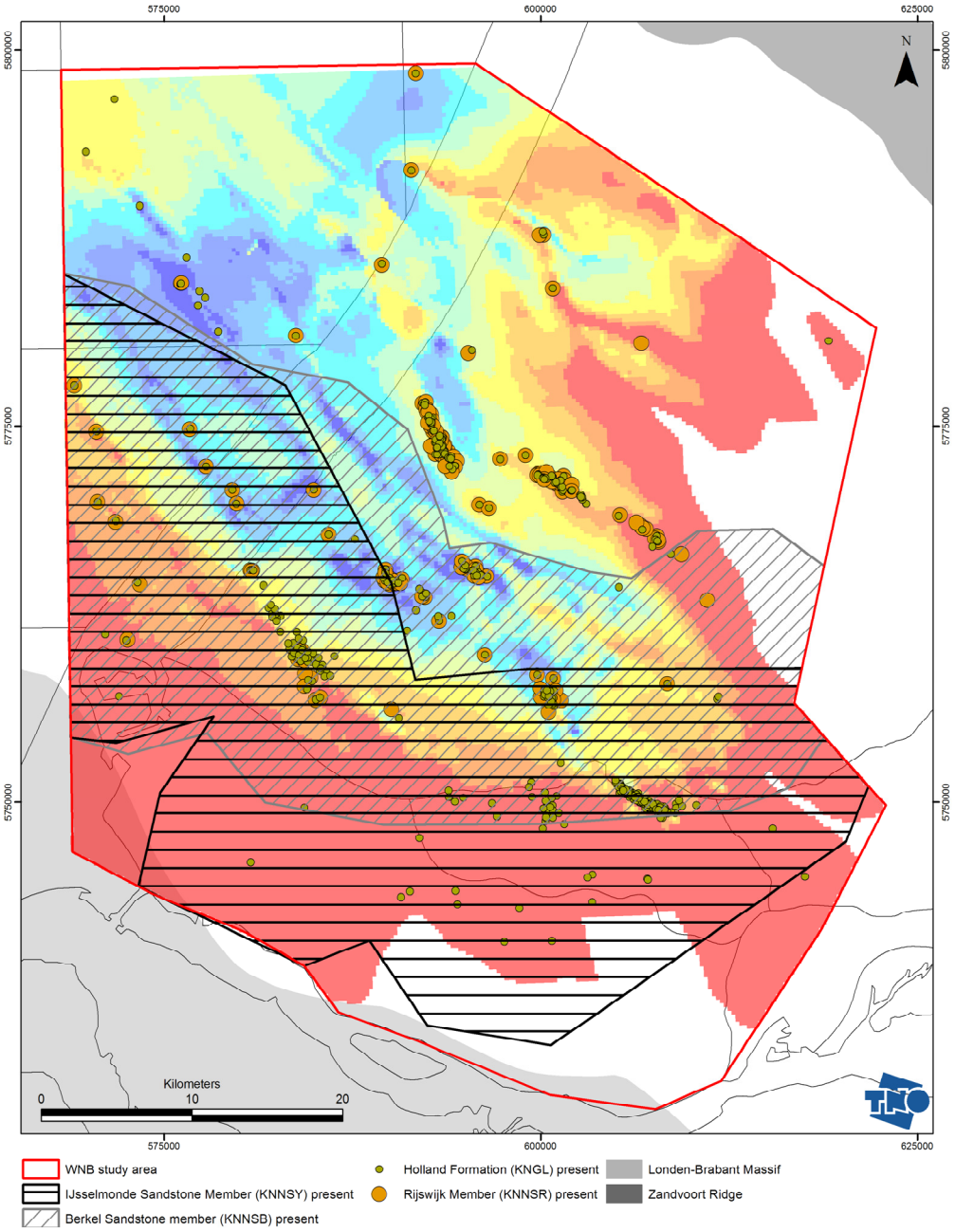

Figure 22. Distribution of lithostratigraphic units in the West Netherlands Basin. The coloured grid reflects the palaeotopography of the basal Rijnland Group surface, where red is high and blue low. See Fig. 1 for location. European Datum 1950, UTM Zone 31N.

A similar distribution has been found before (Racero-Baena and Drake, 1996). The above mentioned members can be seen to migrate landward, especially the barrier complex of the IJsselmonde Sandstone Member is clearly located landward of the Berkel Sandstone Member, in stead of on top of it. This corresponds with the general lithostratigraphy as depicted in Figure 2.

Strikingly, only the Rijswijk Member and the Vlieland Claystone Member are present in the northeast of the WNB. None of the barrier sands (Berkel Sandstone and IJsselmonde Sandstone Members) was encountered there. This cannot be explained by Late Cretaceous erosion, because younger Rijnland Group deposits of the Holland Formation have been preserved (Fig. 22). The absence of barrier sands may be explained by the limited amount of wells in the area. However, based on the palaeotopography and palaeogeography (Ziegler, 1990) of the WNB during the Early Cretaceous, the absence of barrier sands may alternatively be explained by non-deposition in the northeast of the basin. Reasons for this can at this stage only be guessed, but may include (a combination of) the protruding higher elevated topography in the northeast, the limited availability of fluvially supplied sand, and an either large or shallow water depth south of the Zandvoort High, which either hampered shallow marine deposition or barrier formation by breaking waves.

The area with the thickest sand occurrences (Map 1B) corresponds well with the zone in which the Rijswijk, Berkel Sandstone, IJsselmonde Sandstone and De Lier Members occur (Fig. 22).

3.3 Applicability of WNB deposits for geothermal energy

It has already been proven in practice by greenhouse tomato nursery A. en G. van den Bosch B.V. in 2007 in Bleiswijk (www.geothermie.nl) that there is a potential for geothermal energy in the WNB. The net transmissivity maps (Map 3A-D), show areas where the potential for successful wells for geothermal energy is highest. TNO stresses that the maps are the result of a regional-scale study and therefore must not be used to plan wells. The maps can only be used to assist in the evaluation process for estimating the geothermal energy potential of a site. The central part of the WNB between Den Haag, Rotterdam and Gouda has the highest potential for encountering aquifers with sufficient transmissivity in the complete Rijnland Group.

4 Conclusions and recommendations

To improve the understanding of the spatial distribution of Lower Cretaceous aquifers of the Rijnland Group in the West Netherlands Basin, and the suitability of these aquifers for geothermal energy production, a 3D lithofacies model of the basin was constructed. The sand lithofacies in the model were populated with porosity and permeability. Based on the 3D lithofacies, porosity and permeability (transmissivity), net maps were generated. Based on the 3D model and net maps, the following conclusions are drawn:

- The methodology using bulk-data processing, a regional approach, and lithofacies modelling with transmissivity maps as ultimate goal has been successful considering the exploratory nature of this study, the limited amount of data and time and the novelty of the adopted methodology;
- The spatial distribution of aquifers in the 3D model of the Rijnland Group is consistent with general geological concepts and well data for the West Netherlands Basin (in terms of stratigraphic thickness and lateral extent);
- The net sand (aquifer) thickness in the West Netherlands Basin is strongly correlated with the complete thickness of the Rijnland Group. The summed thickness of aquifers is expected to be thickest in the central part of the basin ($\leq$ 500 m) between the cities of Den Haag, Rotterdam and Gouda and thinnest along the basin margins;
- The location of the largest net aquifer thickness corresponds with locations where the Rijswijk, Berkel Sandstone, IJsselmonde Sandstone and De Lier Members occur as stacked sequences;
- The largest net aquifer thickness corresponds with the highest uncertainty of thickness, due to limited well-control in the grabens of the basin;
- No clear permeability trends have been observed in the 3D model, although lowest permeabilities are generally observed at the base of the Rijnland group. This possibly reflects the Rijswijk and Rijn Members;
- Because of largest net aquifer thickness in the central part of the basin, net transmissivity values are highest in that region;
- The facies distribution in the West Netherlands Basin was most likely controlled by the balance between (relative) sea-level rise and fluvial sediment supply;
- The Berkel and IJsselmonde Sandstone Members are absent in the northeast of the West Netherlands Basin. This is tentatively explained by non-deposition as a result of the protruding palaeotopography and a limited supply of (fluvially derived) sand in combination with either a large or very shallow water depth.

In general it can be concluded that the Rijnland Group in the West Netherlands Basin is well suited for geothermal energy production, with emphasis on the central part of the basin between the cities of Den Haag, Rotterdam and Gouda. This study has also resulted in an improved understanding of the data availability and quality in the West Netherlands Basin. Based on that, the following recommendations are made:

- Use and reprocessing of 3D seismic surveys;
- Application of borehole measurements and collection of cores in new wells drilled in the West Netherlands Basin for geothermal energy purposes. This is currently not taking place, unlike the standard procedure for hydrocarbon wells;

- Placement of a new well in a graben or depression where thick sand occurrences in the Schieland Group are expected. This group is under-explored in the grabens and depressions due to the preferential occurrence of hydrocarbons in horst structures;
- A re-evaluation and re-interpretation of stratigraphic well and seismic data of the Schieland Group, to be able to construct a 3D facies model;
- Forward modelling of sand-shale distributions as guidance for 3D facies modelling may considerably improve the understanding of the geology and geological history of the West Netherlands basin.

5 References

Alberts, L.J.H., Geel, C.R. & Klasen, J.J. (2003): Reservoir characterisation using process-response simulations: the Lower Cretaceous Rijn Field, West Netherlands Basin. Netherlands Journal of Geosciences 82: 313-324.

De Jager, J., Doyle, M.A., Grantham, P.J. & Mabillard, J.E. (1996): Hydrocarbon habitat of the West Netherlands Basin. *In:* H.E. Rondeel, D.A.J. Batjes and W.H. Nieuwenhuijs (Eds): Geology of gas and oil under the Netherlands. Kluwer Academic Publishers (Dordrecht): 191-210.

Den Hartog Jager, D.G. (1996): Fluviomarine sequences in the Lower Cretaceous of the West Netherlands Basin: correlation and seismic expression. *In:* H.E. Rondeel, D.A.J. Batjes and W.H. Nieuwenhuijs (Eds): Geology of gas and oil under the Netherlands. Kluwer Academic Publishers (Amsterdam): 229-242.

DeVault, B. & Jeremiah, J. (2002): Tectonostratigraphy of the Nieuwerkerk Formation (Delfland subgroup), West Netherlands Basin. American Association of Petroleum Geologists Bulletin 86: 1679-1707.

Dronkers, A.J. & Mrozek, F.J. (1991): Inverted basins of The Netherlands. First Break 9: 409-418.

Duin, E.J.T., Doornenbal, J.C., Rijkers, R.H.B., Verbeek, J.W. & Wong, T.E. (2006): Subsurface structure of the Netherlands; results of recent onshore and offshore mapping. Netherlands Journal of Geosciences 85: 245-276.

Fridleifsson, I.B., Bertani, R., Huenges, E., Lund, J.W., Ragnarsson, A. & Rybach, L. (2008): The possible role and contribution of geothermal energy to the mitigation of climate change. *In:* O. Hohmeyer and T. Trittin (Eds): IPCC Scoping Meeting on Renewable Energy Sources, Proceedings. IPCC (Luebeck): 59-80.

Geluk, M.C. (1999): Palaeogeographic and structural development of the Triassic in the Netherlands - new insights. *In:* G.H. Bachmann and I. Lerche (Eds): The Epicontinental Triassic - Zentralblatt für Geologie und Paläontology Teil I. - (Halle): 545-570.

Geluk, M.C., Plomp, A. & Van Doorn, T.H.M. (1996): Development of the Permo-Triassic succesion in the basin fringe area, southern Netherlands. *In:* H.E. Rondeel, D.A.J. Batjes and W.H. Nieuwenhuijs (Eds): Geology of gas and oil under the Netherlands. Kluwer Academic Publishers (Dordrecht): 57-79.

Gras, R. & Geluk, M.C. (1999): Late Cretaceous-Early Tertiary sedimentation and tectonic inversion in the southern Netherlands. Geologie en Mijnbouw 78: 1-19.

Haq, B.U., Hardenbol, J. & Vail, P.R. (1987): Chronology of fluctuating sea levels since the Triassic. Science 235: 1156-1167.

Herngreen, G.F.W., Kouwe, W.F.P. & Wong, T.E. (2003): The Jurassic in the Netherlands. *In:* J.R. Ineson and F. Surlyk (Eds): The Jurassic of Denmark and Greenland. Geological Survey of Denmark and Greenland Bulletin (-): 217-229.

Heybroek, P. (1974): Explanation to tectonic maps of The Netherlands. Geologie en Mijnbouw 53: 43-50.

Langenaeker, V. (1998): The Campine Basin, stratigraphy, structural geology, coalification and hydrocarbon potential for the Devonian to Jurassic. Thesis, Katholieke Universiteit Leuven (Leuven): 213 pp.

NITG (2002): Geological Atlas of the subsurface of the Netherlands (1 : 250,000), Explanation to Map Sheet VII and VIII Noordwijk–Rotterdam and Amsterdam-Gorinchem, -. Netherlands Institute of Applied Geoscience TNO (Utrecht): 135 pp.

Racero-Baena, A. & Drake, S.J. (1996): Structural style and reservoir development in the West Netherlands oil province. *In:* H.E. Rondeel, D.A.J. Batjes and W.H.

Nieuwenhuijs (Eds): Geology of gas and oil under the Netherlands. Kluwer Academic Publishers (Dordrecht): 211-228.

Solomon, S., Qin, D., Manning, M., Chen, Z., Marquis, M., Averyt, K.B., Tignor, M. & Miller, H.L. (Eds) (2007): Climate Change 2007: The Physical Science Basis. Contribution of Working Group I to the Fourth Assessment Report of the Intergovernmental Panel on Climate Change. Cambridge University Press, Cambridge, United Kingdom and New York, NY, USA, 996.

Van Adrichem Boogaert, H.A. & Kouwe, W.F.P. (1993): Stratigraphic nomenclature of the Netherlands, revision and update by RGD and NOGEPA. Mededelingen Rijks Geologische Dienst 50: 1-40.

Van Balen, R.T., Bergen, G.v., Leeuw, C.d., Pagnier, H.J.M., Simmelink, H., Wees, J.D.v. & Verweij, J.M. (2000): Modeling the hydrocarbon generation and migration in the West Netherlands Basin, the Netherlands. Netherlands Journal of Geosciences 79: 29-44.

Van Wees, J.D., van Bergen, F., David, P., Nepveu, M., Beekman, F., Cloetingh, S. & Bonté, D. (2009): Probabilistic tectonic heat flow modeling for basin maturation: Assessment method and applications. Marine and Petroleum Geology 26: 536-551.

Van Wijhe, D.H. (1987): Structural evolution of inverted basins in the Dutch offshore. Tectonophysics 137: 171-219.

Worum, G., Michon, L., van Balen, R.T., van Wees, J.-D., Cloetingh, S. & Pagnier, H. (2005): Pre-Neogene controls on present-day fault activity in the West Netherlands Basin and Roer Valley Rift System (southern Netherlands): role of variations in fault orientation in a uniform low-stress regime. Quaternary Science Reviews 24: 473-488.

Ziegler, P.A. (1990): Geological Atlas of Western and Central Europe (2nd edition). Shell Internationale Petroleum Maatschappij B.V.; Geological Society Publishing House (Bath): 239 pp.

6 Signature

Utrecht, Thursday, 29 April 2010
TNO Built Environment and Geosciences

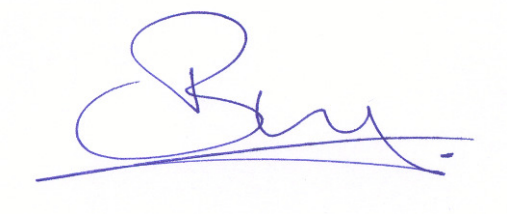

Drs. B.M. Schroot
Head Advisory Group for the Ministry of Economic Affairs

Appendix 1: 538 available wells

1	AHO-E-55	51	DEL-06	101	IJS-23-S1	151	IJS-54-S1	201	LIR-30
2	ALD-01	52	DEL-07	102	IJS-24	152	IJS-55	202	LIR-31
3	ALP-01	53	DEL-08	103	IJS-26	153	IJS-56	203	LIR-32
4	ARV-01	54	EHV-01	104	IJS-28	154	IJS-57	204	LIR-33
5	BLE-01	55	GAG-01	105	IJS-28-S1	155	IJS-57-S1	205	LIR-34
6	BLG-01	56	GAG-02-S1	106	IJS-29	156	IJS-58	206	LIR-35
7	BLG-02	57	GAG-03	107	IJS-29-S1	157	IJS-59	207	LIR-36-S1
8	BRK-01-S1	58	GAG-04	108	IJS-30	158	IJS-60	208	LIR-37
9	BRK-03	59	GAG-05	109	IJS-31	159	IJS-61	209	LIR-38
10	BRK-04	60	GOU-01	110	IJS-31-S2	160	IJS-62	210	LIR-39
11	BRK-05	61	HAG-01	111	IJS-31-S3	161	IJS-63	211	LIR-40
12	BRK-05-S1	62	HAG-02	112	IJS-32	162	IJS-64	212	LIR-41-S1
13	BRK-05-S2	63	HEI-01	113	IJS-32-S1	163	IJS-64-S1	213	LIR-42
14	BRK-06	64	HVS-01	114	IJS-33	164	IJS-65	214	LIR-43
15	BRK-07	65	HZW-01	115	IJS-33-S1	165	IJS-66	215	LIR-44
16	BRK-08-S1	66	IJS-01	116	IJS-34	166	IJS-67	216	LIR-45
17	BRK-08-S2	67	IJS-02	117	IJS-34-S1	167	KDZ-01	217	LIR-47
18	BRK-09	68	IJS-03-S1	118	IJS-35	168	KDZ-02	218	LIR-48
19	BRK-10	69	IJS-04	119	IJS-35-S1	169	LED-01	219	LIR-49
20	BRK-11	70	IJS-04-S1	120	IJS-36	170	LED-02	220	LOD-01
21	BRK-12	71	IJS-05	121	IJS-36-S2	171	LED-03	221	MED-01
22	BRK-13	72	IJS-07	122	IJS-36-S3	172	LEK-01	222	MED-02
23	BRK-14	73	IJS-07-S1	123	IJS-37	173	LIR-01-S3	223	MED-03
24	BRK-15	74	IJS-08	124	IJS-37-S1	174	LIR-02-S1	224	MED-03-S1
25	BRK-16	75	IJS-09	125	IJS-38-S1	175	LIR-03	225	MED-05
26	BRK-17	76	IJS-09-S1	126	IJS-39-S1	176	LIR-04	226	MKP-01
27	BRK-18	77	IJS-10	127	IJS-40	177	LIR-05	227	MKP-02
28	BRK-19	78	IJS-10-S1	128	IJS-40-S1	178	LIR-06	228	MKP-03
29	BRK-20	79	IJS-11	129	IJS-40-S2	179	LIR-07-S1	229	MKP-04
30	BRK-21	80	IJS-12	130	IJS-41-S1	180	LIR-08	230	MKP-05
31	BRK-21-S1	81	IJS-12-S1	131	IJS-42	181	LIR-09	231	MKP-06
32	BRK-22	82	IJS-12-S2	132	IJS-43	182	LIR-10-S1	232	MKP-06-S1
33	BRK-23	83	IJS-13	133	IJS-43-S1	183	LIR-11	233	MKP-08
34	BRK-24	84	IJS-14	134	IJS-44	184	LIR-12	234	MKP-09
35	BRT-01	85	IJS-15-S1	135	IJS-44-S2	185	LIR-13	235	MKP-09-S1
36	BRT-02-S1	86	IJS-15-S2	136	IJS-44-S3	186	LIR-14	236	MKP-10
37	BRT-02-S2	87	IJS-15-S3	137	IJS-45	187	LIR-16	237	MKP-11
38	BRTZ-01	88	IJS-16	138	IJS-45-S1	188	LIR-17	238	MKP-12
39	BRTZ-02-S1	89	IJS-17	139	IJS-46	189	LIR-18	239	MKP-12-S1
40	BRTZ-02-S2	90	IJS-18	140	IJS-46-S1	190	LIR-19	240	MKP-13
41	BRTZ-04	91	IJS-18-S1	141	IJS-47	191	LIR-20	241	MKP-14
42	BSKP-01	92	IJS-19	142	IJS-48	192	LIR-21-S2	242	MKP-15
43	BTL-01	93	IJS-20	143	IJS-48-S1	193	LIR-22	243	MKP-16
44	CAP-01	94	IJS-20-S1	144	IJS-48-S2	194	LIR-23-S1	244	MON-01
45	DEL-01	95	IJS-20-S2	145	IJS-49	195	LIR-24-S1	245	MON-02
46	DEL-02	96	IJS-21	146	IJS-49-S1	196	LIR-25	246	MON-03
47	DEL-03	97	IJS-22	147	IJS-50-S1	197	LIR-26-S2	247	MSG-01
48	DEL-04	98	IJS-22-S1	148	IJS-52	198	LIR-27	248	MSG-02
49	DEL-05	99	IJS-22-S2	149	IJS-52-S1	199	LIR-28	249	MSV-01
50	DEL-05-S1	100	IJS-23	150	IJS-54	200	LIR-29	250	MSV-01-S1

251	MSV-01-S2	301	Q16-01	351	RKK-25	401	RWK-10	451	WAS-17-S1
252	NKK-01	302	Q16-02	352	RKK-26	402	RWK-11	452	WAS-19
253	NKK-02-S1	303	Q16-03	353	RKK-27	403	RWK-12	453	WAS-20
254	NWK-01	304	Q16-04	354	RKK-28	404	RWK-13	454	WAS-21
255	NWK-02	305	Q16-05	355	RKK-29	405	RWK-14	455	WAS-22
256	OAS-01	306	Q16-08	356	RKK-29-S1	406	RWK-15	456	WAS-23
257	OBL-01	307	Q16-FA-101-S1	357	RKK-30	407	RWK-16-S1	457	WAS-23-S1
258	OBLZ-01	308	RDK-01	358	RKK-31	408	RWK-17	458	WAS-23-S2
259	OEG-01	309	RKK-01	359	RKK-32	409	RZB-01	459	WAS-24-S1
260	OLE-01	310	RKK-02	360	RKK-32-S1	410	SCL-01	460	WAS-25
261	PNA-02	311	RKK-03	361	RTD-01	411	SGZ-01-S1	461	WAS-26-S2
262	PNA-03	312	RKK-04	362	RTD-01-S1	412	SGZ-02	462	WAS-27
263	PNA-04	313	RKK-04-S1	363	RTD-02	413	SGZ-04	463	WAS-28-S2
264	PNA-04-S1	314	RKK-04-S2	364	RTD-03-S2	414	SPK-01	464	WAS-28-S3
265	PNA-04-S2	315	RKK-05	365	RTD-04	415	SPKO-01	465	WAS-29
266	PNA-05	316	RKK-06	366	RTD-05	416	SPKO-01-S1	466	WAS-30
267	PNA-06	317	RKK-06-S1	367	RTD-06	417	SPKO-02	467	WAS-30-S1
268	PNA-07	318	RKK-07-S1	368	RTD-07	418	SPKO-02-S1	468	WAS-32
269	PNA-08	319	RKK-07-S2	369	RTD-08	419	SPKW-01	469	WAS-32-S1
270	PNA-09	320	RKK-08	370	RTD-09	420	STR-01	470	WAS-34
271	PNA-10	321	RKK-09	371	RTD-10	421	STW-01	471	WAS-34-S1
272	PNA-11	322	RKK-09-S1	372	RTD-11	422	VAL-01	472	WAS-36
273	PNA-12	323	RKK-09-S2	373	RTD-12	423	VLN-01-S1	473	WAS-37
274	PNA-13	324	RKK-10	374	RTD-13	424	WAS-01	474	WAS-38
275	PNA-14	325	RKK-10-S1	375	RTD-14-S1	425	WAS-02	475	WAS-38-S2
276	PRN-01-S1	326	RKK-11	376	RTD-14-S2	426	WAS-02-S1	476	WAS-39
277	PRW-01	327	RKK-12	377	RTD-14-S3	427	WAS-03	477	WAS-40
278	PRW-02	328	RKK-12-S1	378	RTD-15	428	WAS-04	478	WAS-41
279	PRW-02-S1	329	RKK-12-S2	379	RTD-15-S1	429	WAS-04-S1	479	WAS-42
280	PRW-03-S2	330	RKK-12-S4	380	RTD-16	430	WAS-05	480	WAS-42-S1
281	PRW-04	331	RKK-13	381	RTD-16-S2	431	WAS-06	481	WAS-43-S1
282	PRW-05	332	RKK-14	382	RTD-17	432	WAS-06-S1	482	WAS-44
283	PRW-06	333	RKK-14-S1	383	RTD-18	433	WAS-07	483	WAS-44-S2
284	Q13-01	334	RKK-14-S2	384	RTD-18-S1	434	WAS-07-S1	484	WAS-45
285	Q13-02	335	RKK-15	385	RTD-18-S2	435	WAS-07-S2	485	WAS-46
286	Q13-03	336	RKK-15-S1	386	RTD-19	436	WAS-08	486	WAZ-01
287	Q13-04	337	RKK-15-S2	387	RTD-19	437	WAS-08-S1	487	WOB-01
288	Q13-04-S1	338	RKK-16	388	RTD-19-S1	438	WAS-09	488	ZOM-01
289	Q13-05	339	RKK-17	389	RTD-20	439	WAS-09-S1	489	ZOM-02
290	Q13-06	340	RKK-17-S1	390	RTD-20-S1	440	WAS-10	490	ZOM-02-S1
291	Q13-07	341	RKK-17-S2	391	RTD-21	441	WAS-10-S3	491	ZOM-03
292	Q13-07-S1	342	RKK-18	392	RWK-01	442	WAS-10-S4	492	ZOM-04
293	Q13-07-S2	343	RKK-19	393	RWK-02	443	WAS-10-S5	493	ZOM-05
294	Q13-08	344	RKK-20	394	RWK-03	444	WAS-12	494	ZOM-06
295	Q13-09	345	RKK-21	395	RWK-04	445	WAS-13	495	ZOM-06-S1
296	Q13-10	346	RKK-22	396	RWK-05	446	WAS-14	496	ZOM-07
297	Q13-11	347	RKK-23	397	RWK-06	447	WAS-15	497	ZOM-08
298	Q14-01	348	RKK-23-S1	398	RWK-07	448	WAS-15-S1	498	ZOM-09
299	Q14-02	349	RKK-24	399	RWK-08	449	WAS-16	499	ZOM-10
300	Q14-03	350	RKK-24-S1	400	RWK-09	450	WAS-17	500	ZOM-10-S2

501	ZOM-12
502	ZOM-12-S1
503	ZOM-13
504	ZOM-14-S1
505	ZOM-15
506	ZOM-15-S1
507	ZOM-16
508	ZOM-16-S1
509	ZOM-17-S1
510	ZOM-18
511	ZOM-19
512	ZOM-20
513	ZOM-20-S1
514	ZOM-21-S1
515	ZOM-21-S2
516	ZOM-22
517	ZOM-23
518	ZOM-24
519	ZOM-24-S1
520	ZOM-24-S2
521	ZOM-26
522	ZOM-27
523	ZOM-27-S2
524	ZOM-28
525	ZOM-29
526	ZOM-30
527	ZOM-31
528	ZOM-32
529	ZOM-33
530	ZOM-34
531	ZOM-35
532	ZOM-36-S1
533	ZOM-37
534	ZOM-38
535	ZOM-38-S1
536	ZOM-39
537	ZOM-40
538	ZOM-40-S1

Appendix 2: facies analysis

Cluster analysis

Cluster analysis of the available well logs, indicated that the use of extra logs (such as neutron, density and sonic logs) would not contribute to a significantly better division of the lithofacies when compared with the gamma ray (GR) log.

Cluster analysis is "an exploratory data analysis tool, which aims at sorting objects into groups in a way that the degree of association between two objects is maximal if they belong to the same group and minimal otherwise (definitions at www.statsoft.com/textbook/stcluan.html)". The implemented cluster analysis method was K-means clustering. In short, this method works as follows: "Given a fixed (K) number of clusters, assign observations to those clusters so that the means across clusters (for all variables) are as different from each other as possible[1]".

Wells used for the cluster analysis were: Botlek-01, Gaag-05, Monster-02, Q13-08 and Q13-09. As this analysis showed that no extra insights would be gained by using other kinds of logs and because the GR log is the most readily available log, lithofacies have only been divided by using GR.

Map 1A: net sand lithofacies thickness map (P10) of the Rijnland Group in the West Netherlands Basin

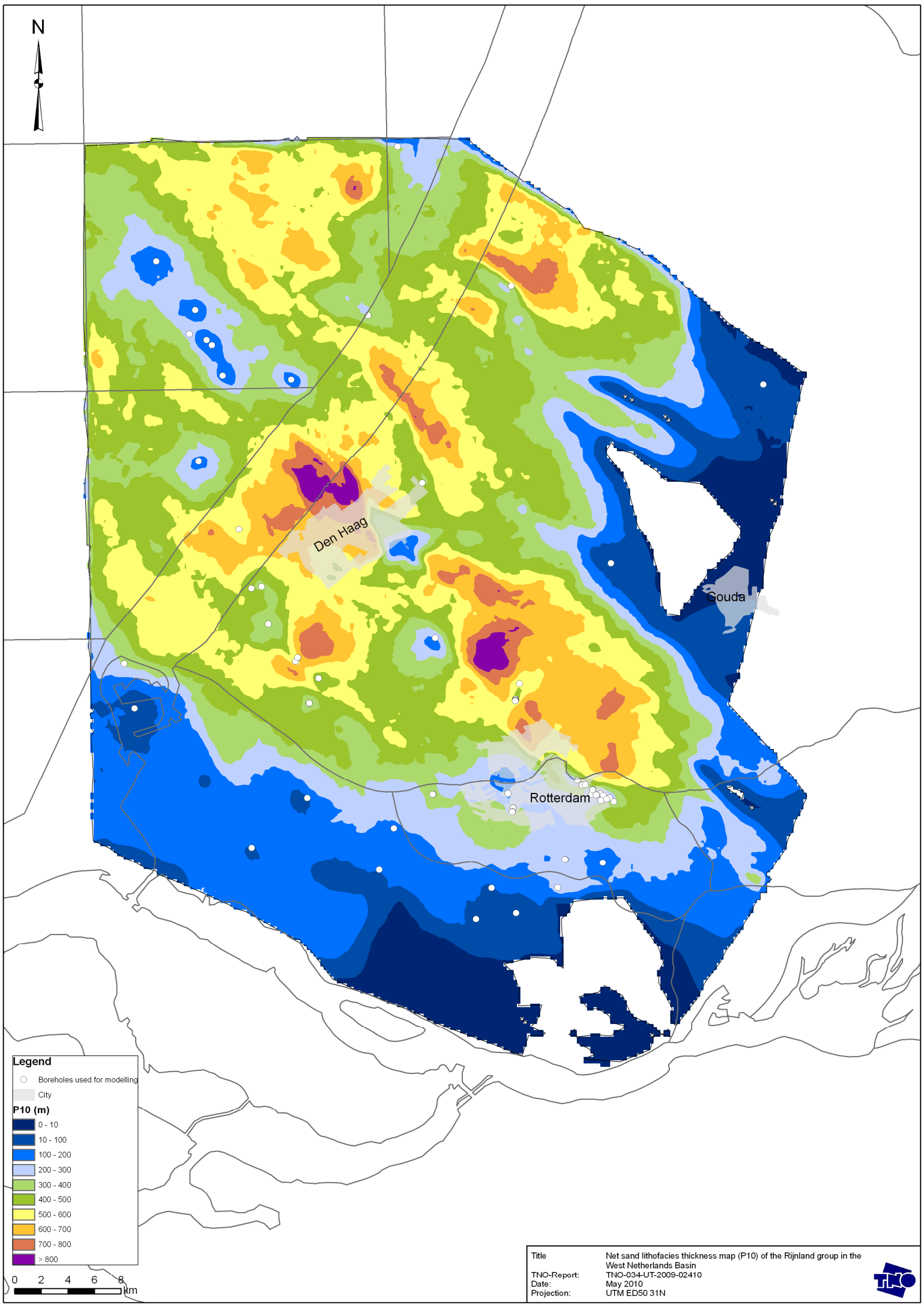

Map 1B: net sand lithofacies thickness map (P50) of the Rijnland Group in the West Netherlands Basin

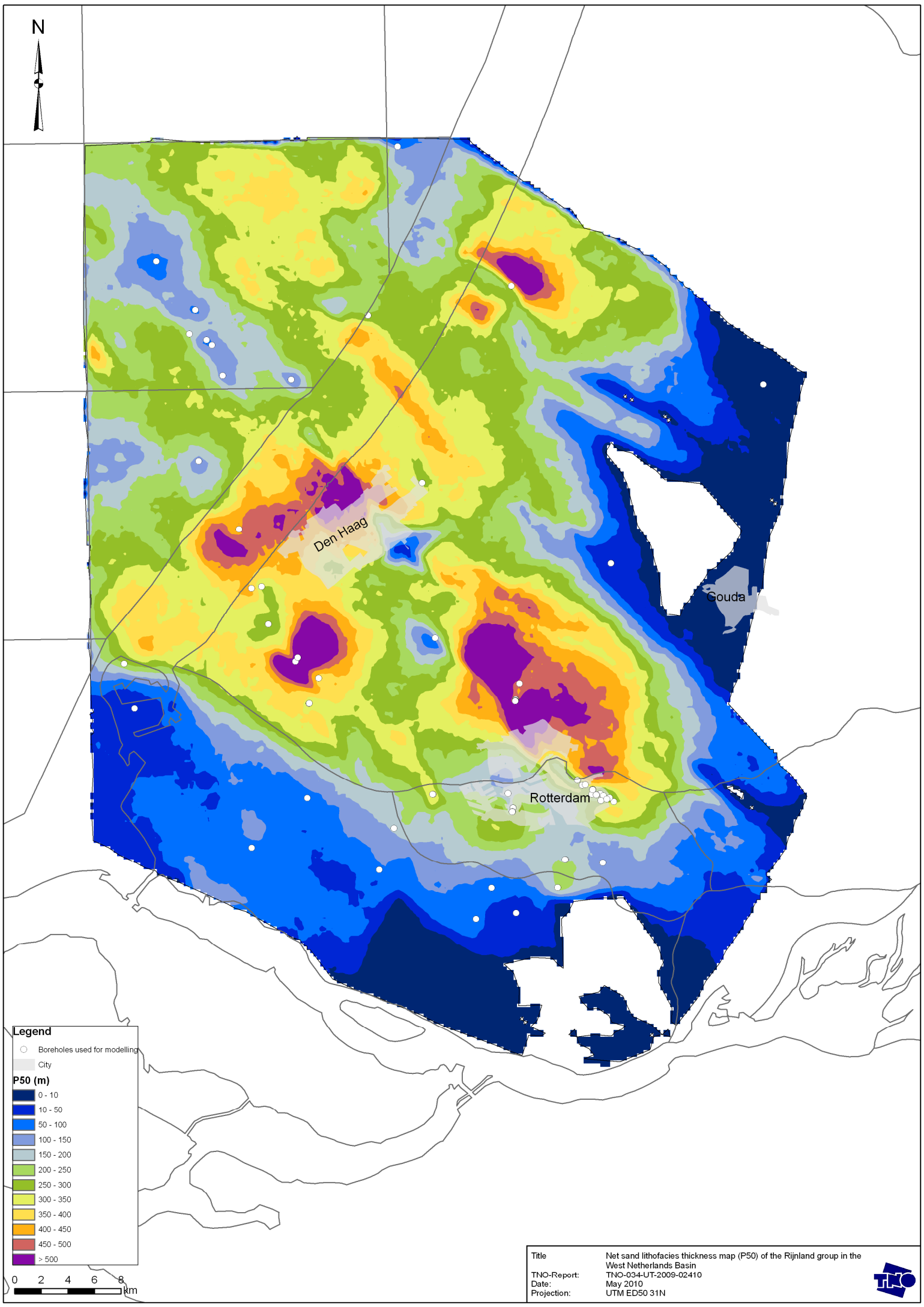

Map 1C: net sand lithofacies thickness map (P90) of the Rijnland Group in the West Netherlands Basin

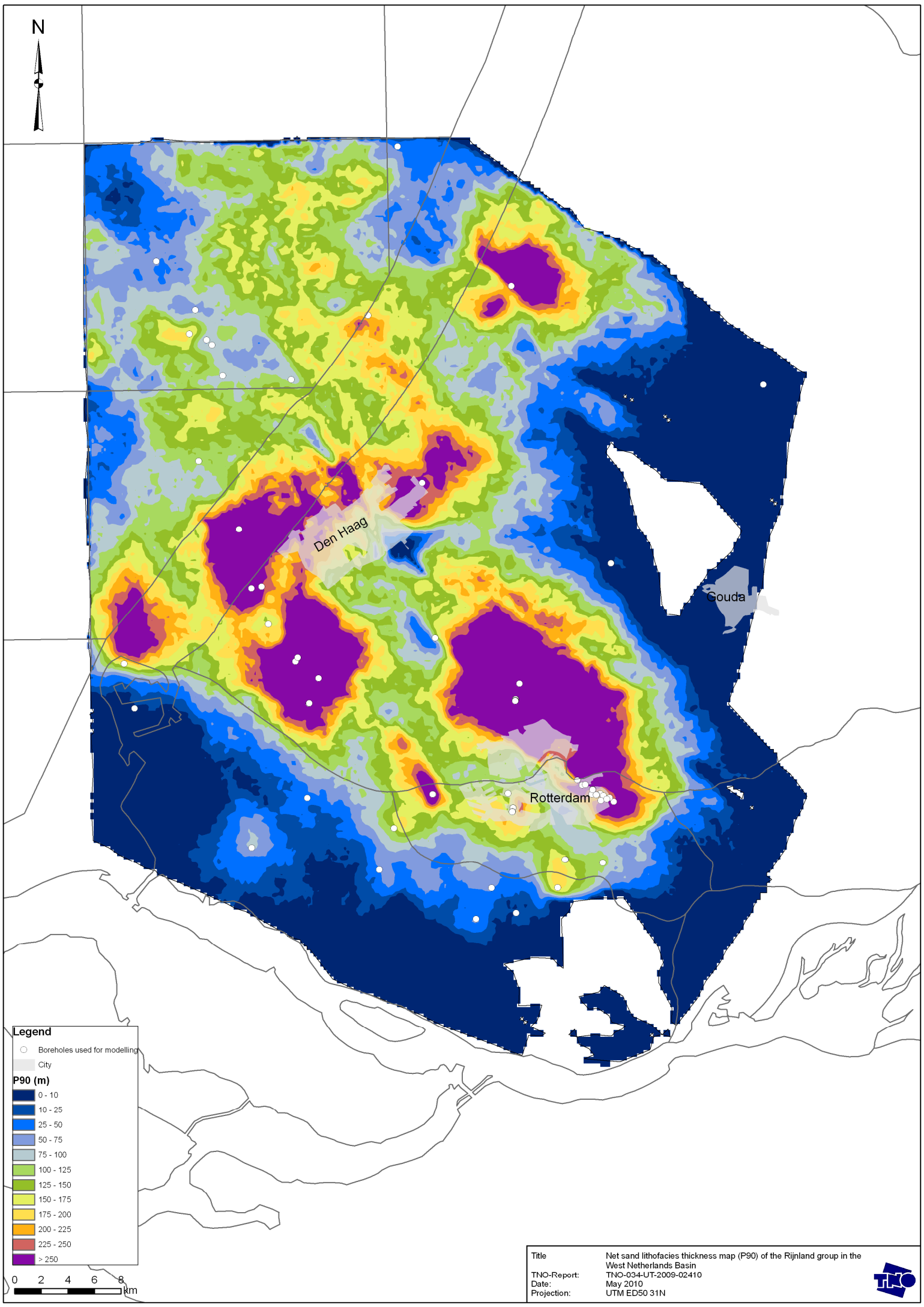

Map 1D: net sand lithofacies thickness map (P10-P90) of the Rijnland Group in the West Netherlands Basin

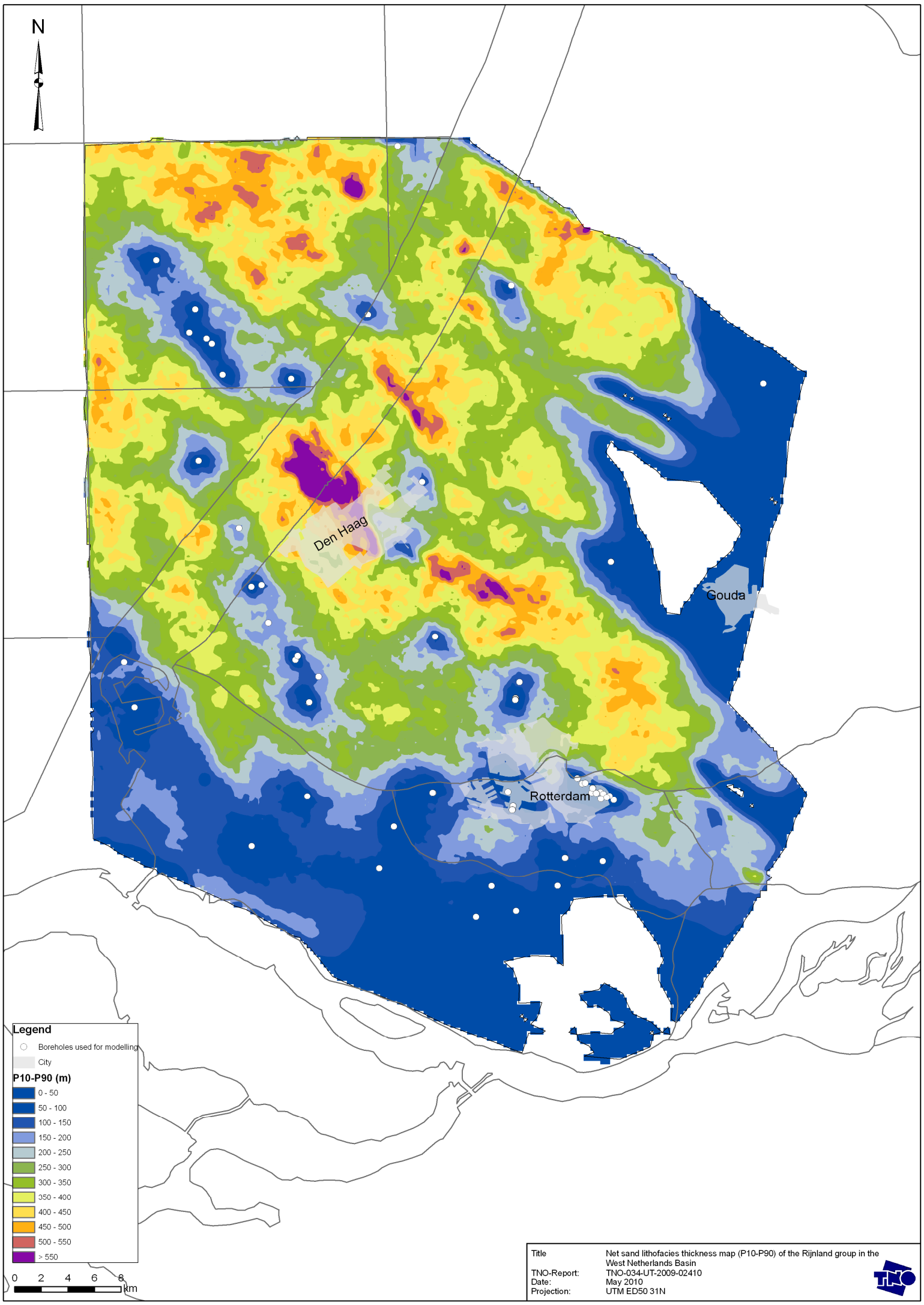

Map 2A: net porosity map (P10) of the Rijnland Group in the West Netherlands Basin

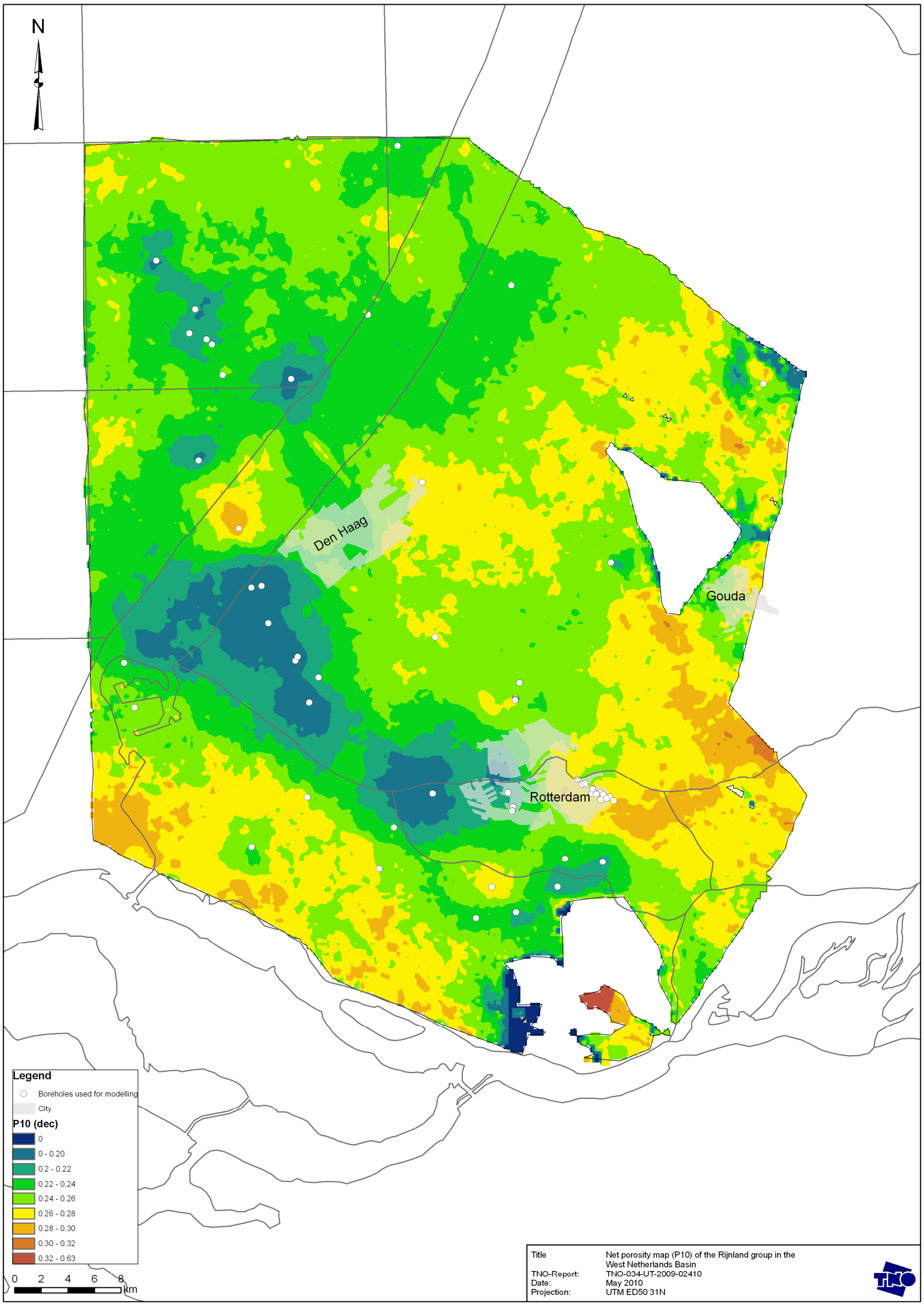

Map 2B: net porosity map (P50) of the Rijnland Group in the West Netherlands Basin

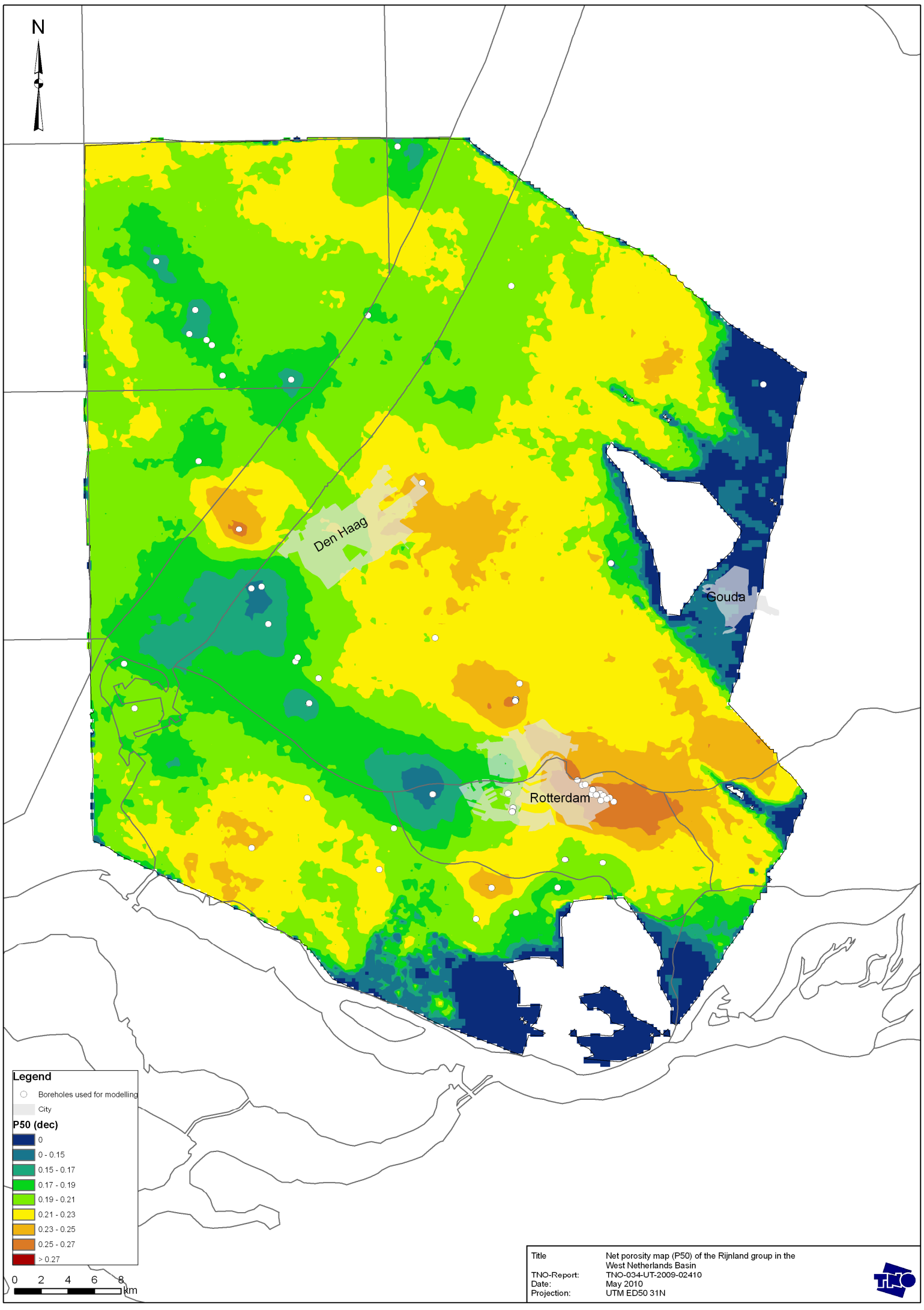

Map 2C: net porosity map (P90) of the Rijnland Group in the West Netherlands Basin

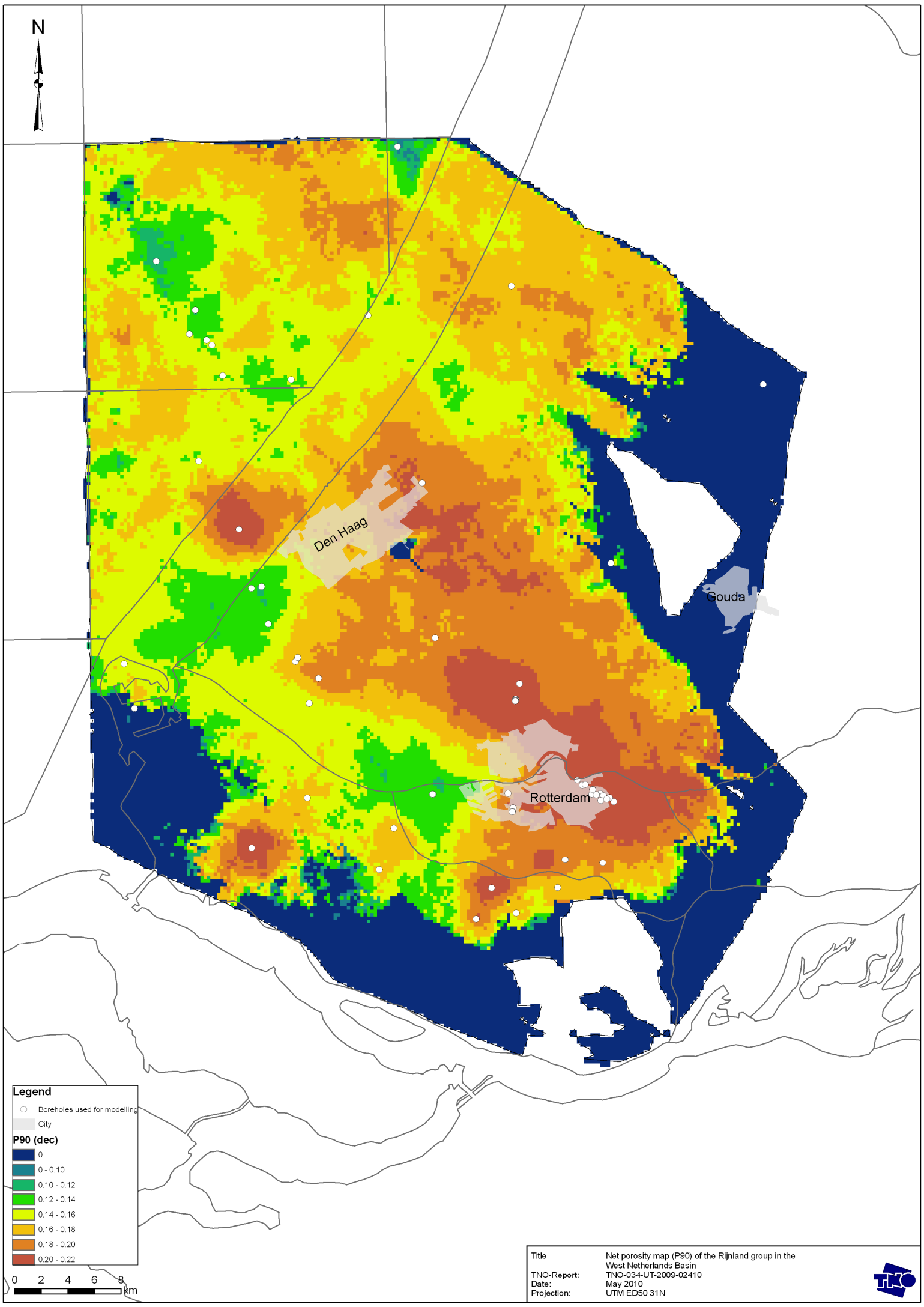

Map 2D: net porosity map (P10-P90) of the Rijnland Group in the West Netherlands Basin

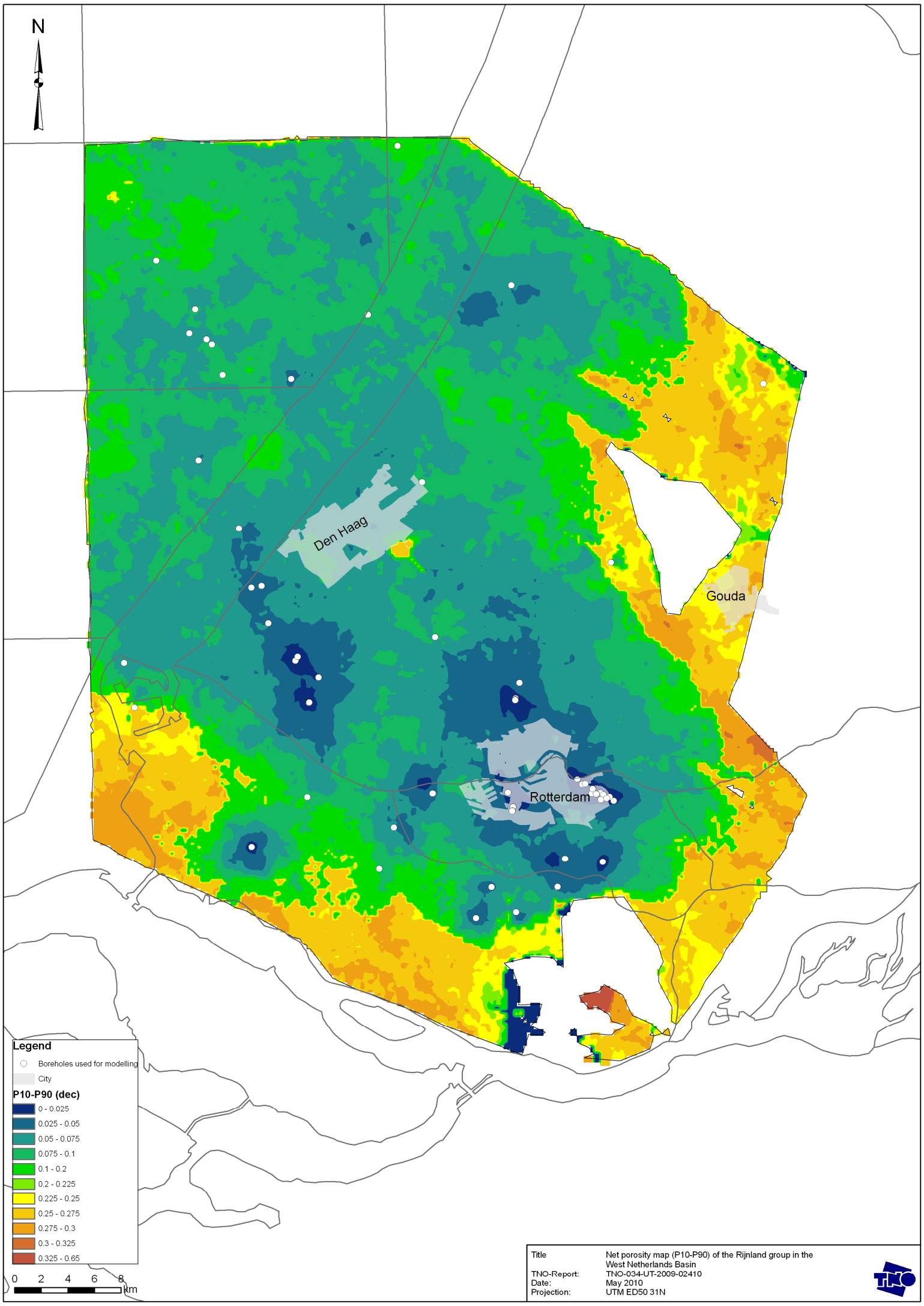

Map 3A: net transmissivity map (P10) of the Rijnland Group in the West Netherlands Basin

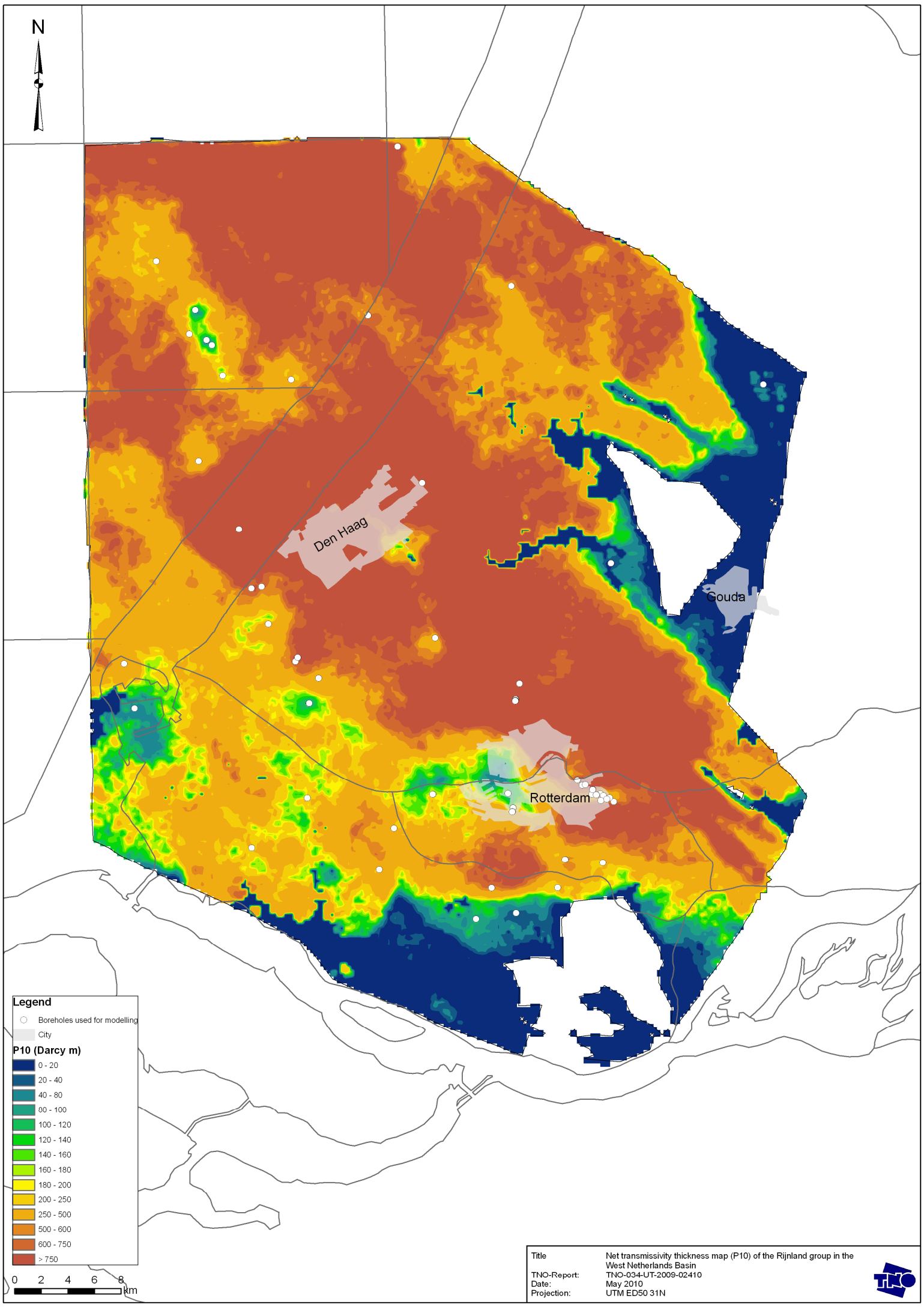

Map 3B: net transmissivity map (P50) of the Rijnland Group in the West Netherlands Basin

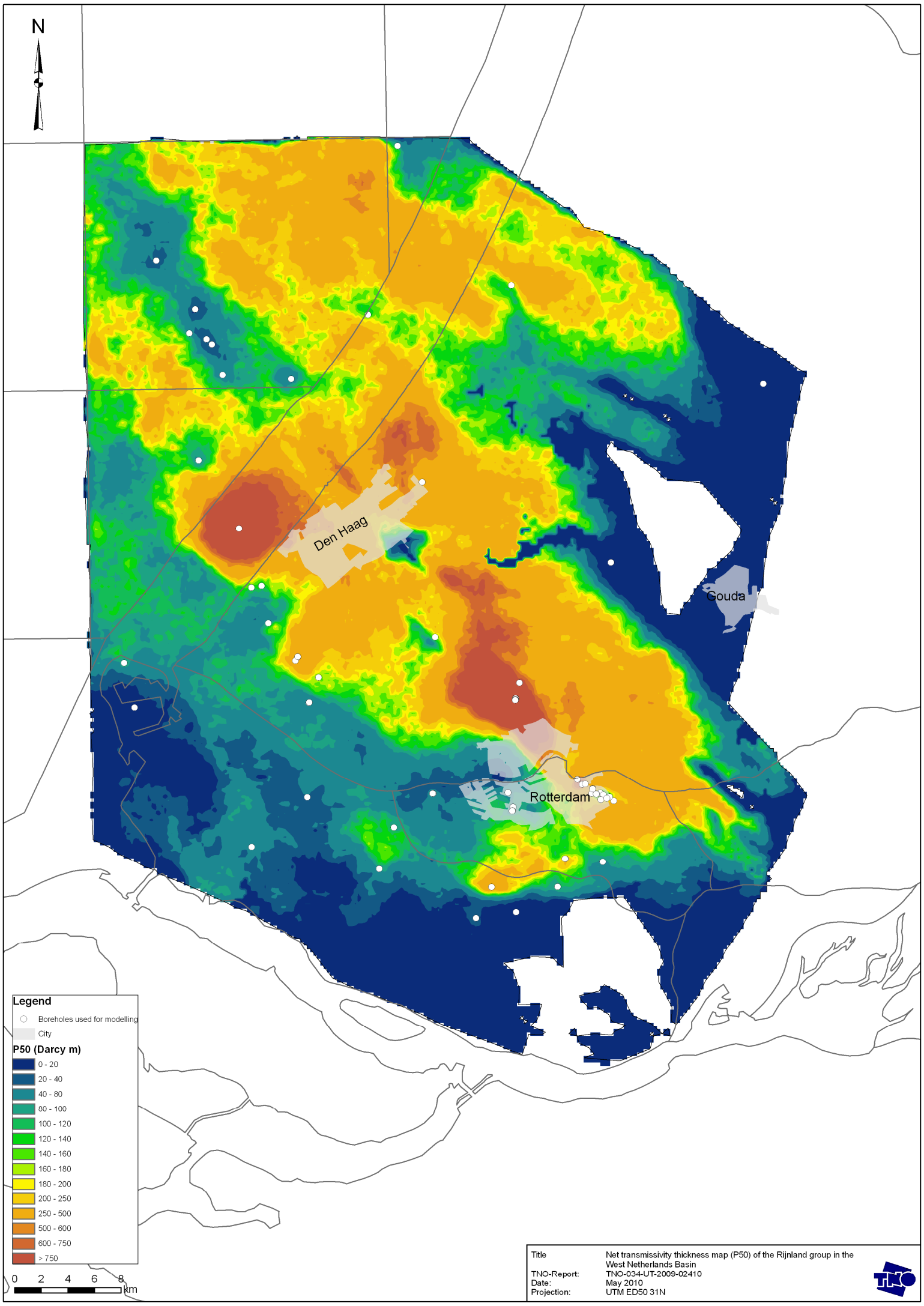

Map 3C: net transmissivity map (P90) of the Rijnland Group in the West Netherlands Basin

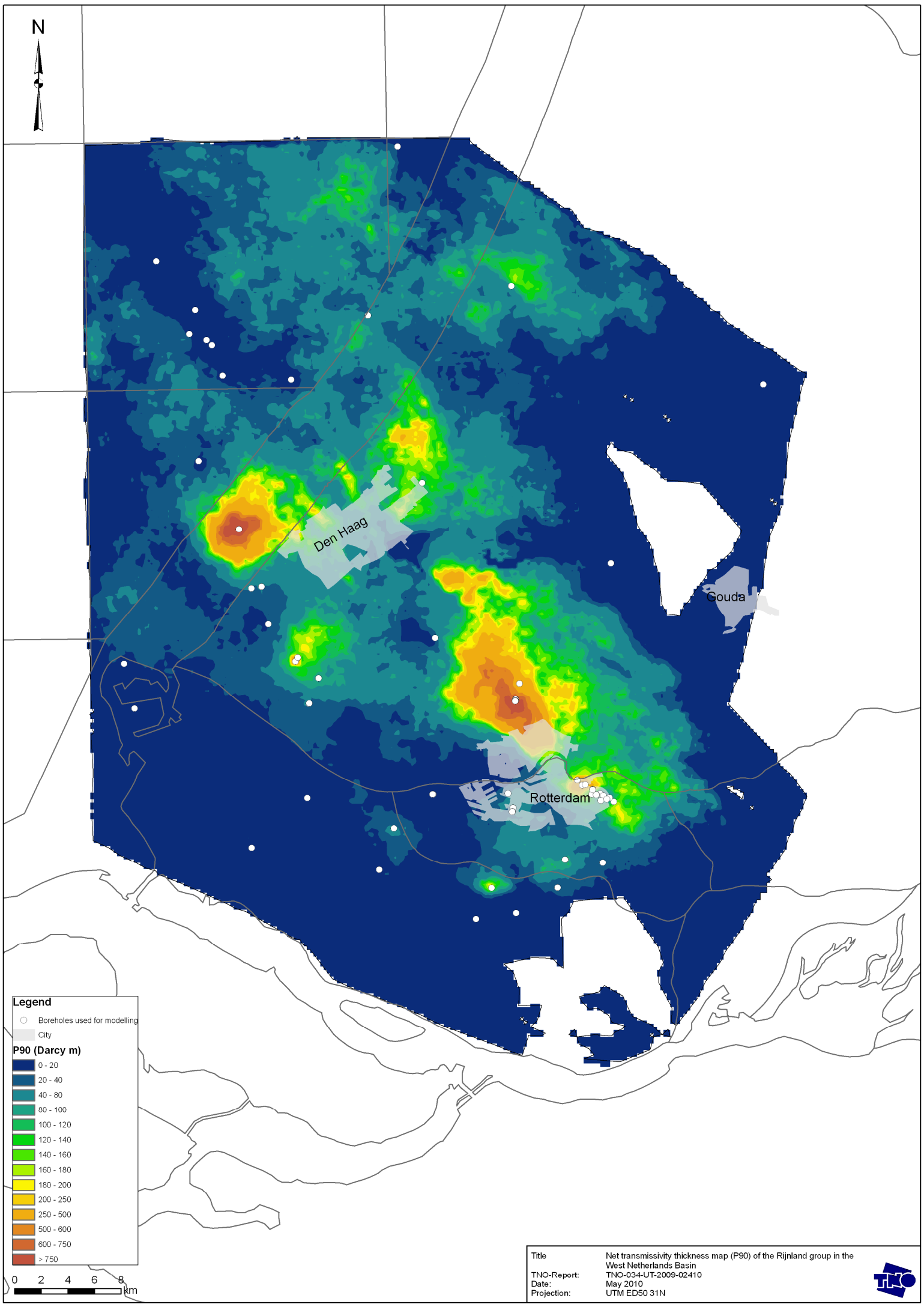
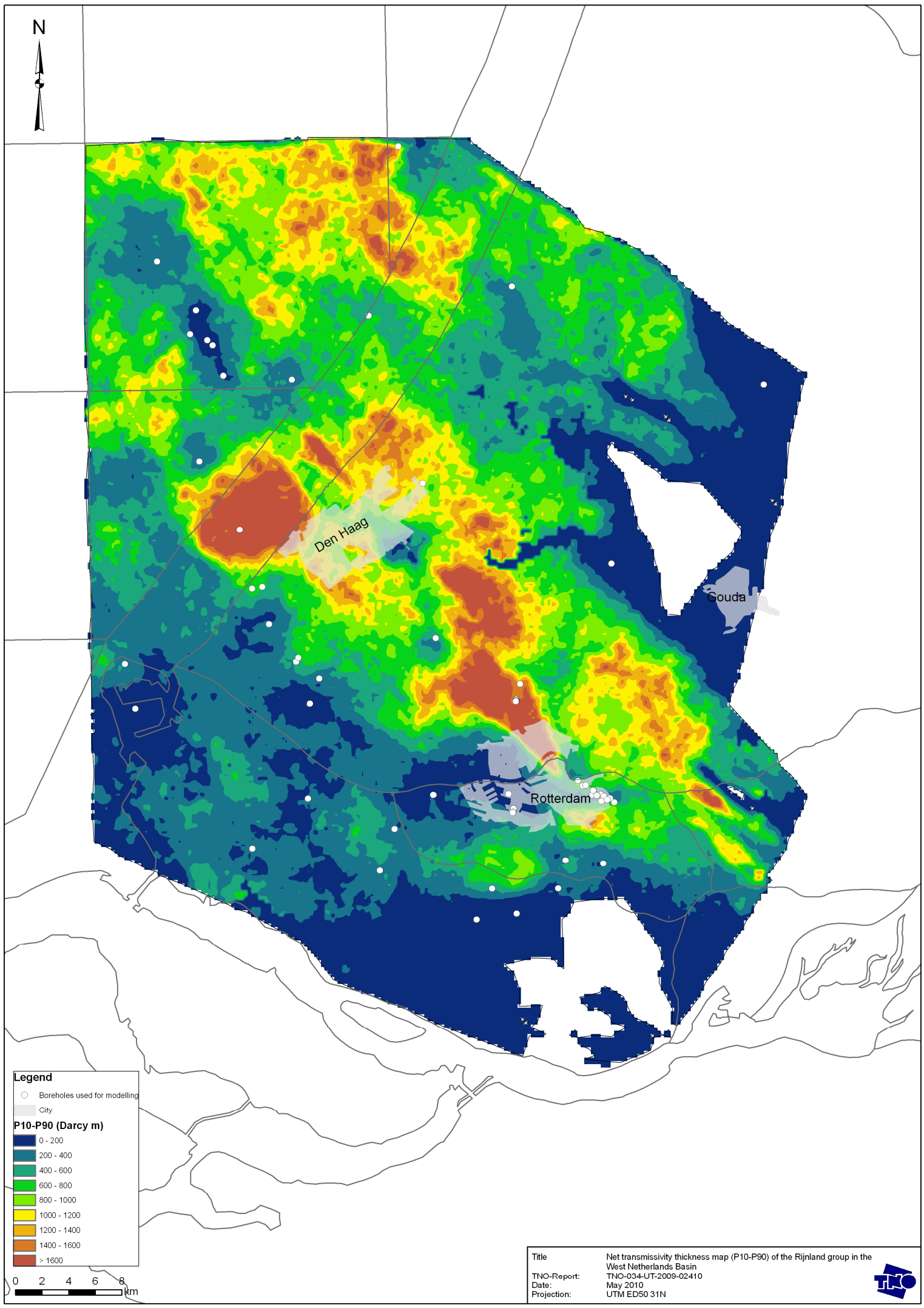
Map 3D: net transmissivity map (P10-P90) of the Rijnland Group in the West Netherlands Basin